Timing Analysis of X-ray binaries

A Thesis

submitted to
Indian Institute of Science Education and Research Pune
in partial fulfillment of the requirements for the
BS-MS Dual Degree Programme

by

Nandini Hazra

Indian Institute of Science Education and Research Pune
Dr. Homi Bhabha Road,
Pashan, Pune 411008, INDIA.

December, 2018

Supervisor: Prof. Dipankar Bhattacharya

© Nandini Hazra 2018

All rights reserved

Certificate

This is to certify that this dissertation entitled Timing Analysis of X-ray binaries towards the partial fulfilment of the BS-MS dual degree programme at the Indian Institute of Science Education and Research, Pune represents study/work carried out by Nandini Hazra at Indian Institute of Science Education and Research under the supervision of Prof. Dipankar Bhattacharya, Professor, IUCAA, Pune , during the academic year 2018-2019.

Prof. Dipankar Bhattacharya

Committee:

Prof. Dipankar Bhattacharya

Dr. Prasad Subramanian

This thesis is dedicated to my mother

Declaration

I hereby declare that the matter in the report titled Timing Analysis of X-ray binaries is the result of the work carried out by me at IUCAA, Pune, under the supervision of Prof. Dipankar Bhattacharya and the same has not been submitted elsewhere for any other degree.

Nandini Hazra

Nandini Hazra

Acknowledgments

I would like to thank my advisor, Dr Dipankar Bhattacharya, for his guidance, unending patience and faith in me, which has kept me anchored throughout this year. I also thank Dr Prasad Subramanian for his support, ideas, feedback and encouragement. I also express my gratitude towards Dr Tomaso Belloni for his insight, ideas and arguments, and to Dr Bhas Bapat and Dr Ramana Athreya for always having time and advice for me. I thank Yash Bhargava, Suman Bala, Anjali Rao, Jayashree Roy and Md Shah Alam at IUCAA for always helping me when I was stuck. Finally, I would like to thank my mother for her unconditional support, and my friends for coffee and conversations.

Abstract

Timing and spectral analysis can give us valuable information about the properties of a compact binary system, by studying the evolution of its parameters throughout the course of an observation or within sections of a single pulse. GX 301-2 is a neutron star belonging in a high mass X-ray binary. It has a pulse spin period of about 686 seconds, and revolves around its companion Wray 977 (a B-type supergiant) in a highly eccentric orbit ($e = 0.47$), while accreting mass from the supergiant's stellar wind. It has known to show flare ups at the pre-periastron when it passes through the dense stellar wind close to the Be disc.

In this project, we have taken an observation from May 2010, when GX 301-2 was just in the post-apastron region of its orbit. The light curve of GX 301-2 showed an anomalous dip in its pulse, lasting for a very brief time- exactly 1 pulse period. The brevity of the dip as well as certain spectral characteristics leading up to it make it a very novel and interesting problem. We discuss why this is interesting, and perform timing and spectral analysis on this chunk of data to determine what the cause of such a dip could be.

Contents

Abstract **vi**

1 Introduction **1**

1.1 X-ray binaries and accretion 1

1.2 Timing Analysis 2

2 The problem at hand **4**

2.1 Describing the system : GX 301-2 4

2.2 Observation of an anomalous dip 6

2.3 The instrument used : RXTE/PCA- Details and Data modes 7

3 Process of data reduction used **9**

3.1 Selecting the data files 9

3.2 Barycentric correction 10

3.3 Good Time Intervals 10

3.3.1 Number of PCUs 11

3.3.2 Elevation 12

3.3.3 Offset 13

3.3.4 Time since South Atlantic Anomaly 14

3.3.5 Electron contamination 16
3.4 Generating background 17
3.5 Generating response 17
3.6 Obtaining the light curves and spectra 18

4 Analysis **19**
4.1 Preliminary analysis for the entire observation 19
4.1.1 Fitting a model to the spectrum 19
4.1.2 Finding the pulse period 20
4.2 Analysing each pulse 23
4.3 Analysing component pulses before and after the dip 31

5 Discussion **34**
5.1 Previously discussed phenomena 34
5.1.1 Absorption by interstellar gas clouds 34
5.1.2 Propeller effect 35
5.1.3 Brief stop in accretion flow 36
5.2 Our hypotheses 36
5.2.1 Occlusion by opaque object 37
5.2.2 Magneto-hydrodynamic instability 37
5.2.3 Geometry of the beam 39

6 Conclusion **40**

7 Appendix : A **41**
7.1 The Detectors on Astrosat 41

7.2 The Object : Crab 42

7.3 Step 1 : Pipeline 42

7.4 Step 2 : Barycentric Correction 42

7.5 Step 3 : Use the spectra/lightcurves 43

7.5.1 Do a spectral fitting 43

7.5.2 Lightcurves 44

7.5.3 Phase resolved spectroscopy 48

List of Figures

2.1 A rought sketch of GX 301-2 5

2.2 The anomalous dip observed by Göğüş et al. on May 28, 2010 6

3.1 Number of PCUs that are recording events throughout the duration of our observation 11

3.2 GoodXenon events from PCU 2, 3 and 4 12

3.3 Elevation of the target with respect to the Earth's limb 13

3.4 Offset in the pointing of the satellite with respect to the target's position . . 14

3.5 The Van Allen Radiation belt 14

3.6 Elevation of the target with respect to the Earth's limb 15

3.7 Elevation of the target with respect to the Earth's limb 16

4.1 The full lightcurve, the power spectrum and a single pulse 21

4.2 Efsearch results 22

4.3 First 4 pulses 23

4.4 Pulses 5-10 24

4.5 Last 4 pulses 25

4.6 A sample fit for the 1st pulse 26

4.7 A sample fit for the 1st pulse, with systematic error added 27

4.8 The iron line centroid 28

4.9 The hydrogen column depth 29

4.10 The photon index 29

4.11 Modulation fraction 30

4.12 The 6th pulse, with 16 s bins 31

4.13 Break energy for all the fits 32

4.14 A sample fit using broken power law : the primary pulse post dip 32

4.15 Photon index 1 33

5.1 Viscous timescale 36

5.2 Magnetohydrodynamic instability in accretion 38

5.3 Critical mass accretion rate for MHD instability 38

7.1 Spectral fitting for obs id 620, and Parameters for fit to obs id 620 (background systematic error 5%, Model systematic error 2% 45

7.2 Power spectrum for Crab 46

7.3 Result of efsearch for Crab 47

7.4 Epoch folded lightcurve for Crab 47

Chapter 1

Introduction

1.1 X-ray binaries and accretion

X ray binaries are broadly classified into two families- the HMXB (High Mass Xray Binaries) and the LMXB (Low Mass Xray Binaries), depending on the mass of the primary object. In the systems we study, the primary object accretes mass from the companion star. There are two principal mechanisms by which this occurs :

1. Roche lobe overflow : The Roche Lobe in a binary system is an area bounded by a critical gravitational equipotential surface around both the objects in the binary, which intersect at the Lagrangian 1 point between the two. It is a dumb-bell shaped region, within which matter is gravitationally bound to the system. Due to several reasons like rapid expansion of the companion star due to nuclear evolution, or due to orbital evolution causing shrinking of lobes, or sometimes angular momentum loss due to gravitational waves, the companion star fills out its Roche lobe and this causes what is called a Roche Lobe Overflow.

2. Stellar Wind : This is more commonly seen in binaries with an early type massive star (O or B type) companion and a neutron star primary. However, there are exceptions to this, like Cygnus X1, where the primary is a black hole and the accretion is believed to be through stellar wind. This method of accretion is much less efficient than Roche lobe overflow, as the wind flows out from the companion in all directions and only a fraction of it is intercepted by the compact primary object.

The accreted matter usually forms a disk around the primary object, perpendicular in plane to the axis of rotation of the compact object. To conserve angular momentum, the infalling material should lose angular momentum as its orbit shrinks. To compensate for this, some matter should move outward. This generates viscous forces in the disc, and the friction ultimately causes the gas to heat up and release radiation in the X-ray band. Alternatively, as the accreted matter gets close to a black hole, it starts getting vigorously sucked in by the gravity and this can also cause friction and the release of X-ray jets.

1.2 Timing Analysis

Let's talk a little bit about the relevance of Timing studies for X-ray binaries. X ray binaries are transient sources, and periodically or quasi-periodically, peak in intensity by a huge factor (over 100). We can do spectral and temporal studies of these pulses to extract certain information about the binary system.

The study of lightcurves can tell us a lot about a pulsar. We can determine the period of its rotation by determining the periodicity of the peaks in the lightcurve. We can also understand if it is orbiting around another object by doppler shifts, and we can also tell if it is being eclipsed by its companion, if there is a periodic drop in the flux whose period differs from that of the pulsar rotation.

On the other hand, spectral analysis gives us information regarding the temperature, photon index, nature of the accretion disk (if it is optically thick or thin, the temperature of electrons, etc.) by fitting of different models to the spectra. We can also determine how these parameters change in different energy bands, which can also give us a clue as to what physical processes are going on in the accretion disk. Sometimes it also gives us a clue regarding element abundances and magnetic field around the primary.

In tandem, lightcurves and spectra can be used to do phase-resolved spectroscopy, in which the spectra of different parts of the lightcurve pulse periodic unit can be studied by assigning it a phase, and fitting each part separately.

For this project, I started out trying to learn the various techniques by which we can extract information from a set of X ray data, using timing and spectral analysis. For this, I used data for a standard object- the Crab pulsar, which is easy to characterise because of its brightness and simple power law trend in its energy spectrum. We used data from Astrosat LAXPC. The analysis carried out has been appended in the Appendix A, and the techniques learned have been used for the following part.

Chapter 2

The problem at hand

2.1 Describing the system : GX 301-2

GX 301-2 is a high mass X-ray binary system comprised of an accreting neutron star and a B1 Ia+ type supergiant star companion called Wray 977. The two components are in a highly eccentric orbit (e= 0.47 [1]) around each other and the pulsar is powered by the stellar wind from Wray 977. It has been established that the Roche lobe of the companion is underfilled, and the hypothesis that the stellar wind drives the accretion is supported by the accretion rate of the neutron star. The accretion happens via a combination of the neutron star intercepting matter from the stellar wind, as well as from a spiral gas stream from the companion near the apastron. The interception of the stellar wind near the periastron causes a flare up in the X-ray pulse just before the periastron [1] Figure 2.1.

The orbital period of the neutron star is about 41.5 days, and the spin period of the NS itself is 686 s. However, the object has gone through several spin-up and spin-down episodes which causes its spin period to vary. The accreting matter is believed to be clumpy in the stellar wind away from the NS, due to the temporal variability in H1 column densities calculated. Close to the poles of the NS, the accreting matter forms a column which rises out high above the poles.

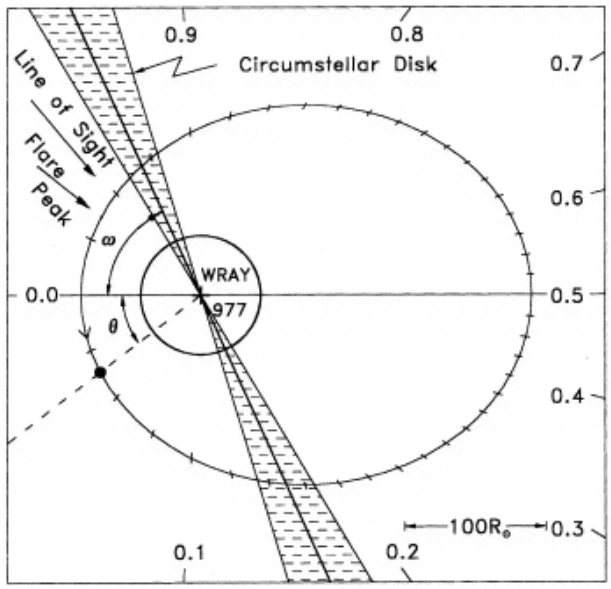

Figure 2.1: A rought sketch of GX 301-2. The markings on the square border denote the orbital phase, and the projection onto the orbit is denoted by the markings on the elliptical orbit. It also shows us the line of sight direction and the approximate location of the circumstellar disc. source : [2][3]

A lot of the spectral behaviour of GX 301-2 is seen to be similar to Vela X-1, and the two are often compared while looking at accretion mechanisms and spectral anomalies. The continuum of GX 301-2 is described using an absorbed power law with a Fermi Dirac cutoff in the 20-30 keV range. Alternatively, a best fit high energy cutoff or a negative-positive exponential fit (NPEX) are used to fit the continuum. Additionally an iron K-edge line is seen at 6-7 keV, which is usually a combination of the Kα and Kβ edge absorption features. Around 35 keV, we can also see a highly variable cyclotron resonance scattering feature (CRSF) that varies in centroid energy and width quite drastically. The centroid energy can be used to estimate the magnetic field of the NS in GX 301-2, and comes out to be of the order of 10^{12} G. (However, in our data, we don't have enough signal to noise ratio at 35 keV to observe the CRSF).

The pulse profile of the NS looks like a regular pulsar with two peaks of varying intensity. The peaks differ in relative intensities and well as absolute intensities at different energy bands.

2.2 Observation of an anomalous dip

In 2011, Gogus et. al discovered what they called a "peculiar dip"[4] in the signal from GX 301-2, observed using the Rossi X-ray Timing Explorer, which lasted for the duration of 1 spin period of the neutron star- roughly 686 s. The observations, as they calculated using the Doroshenko 2010 ephemeris [5], were close to the orbital phase 0.7, which coincides with the post-apastron part of the orbit of GX 301-2 around Wray 977. They ruled out absorption being a cause of the dip, and briefly discuss the timescale of the event not being consistent with timescales of propeller effect or a radical decrease of accretion flow, which could cause such a dip. The exact correspondence of the dip to 1 spin period and the very short timescale of its occurence makes it a very interesting and unique phenomenon.

We will perform timing and spectral analysis for a section of the data leading up to and after this dip. The length of the observation we have considered is about 10 ks, and we have used the same data from the RXTE GOF archives as Gogus et al (Proposal ID 95354-03-03-00), and focused on the Good Xenon event files from the Proportional Counter Array.

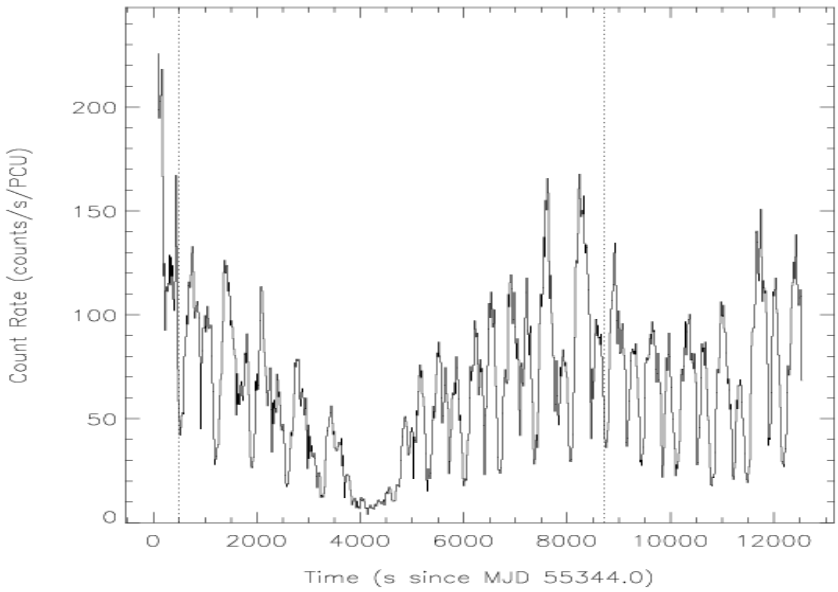

Figure 2.2: The anomalous dip observed by Göğüş et al.[4] on May 28, 2010

2.3 The instrument used : RXTE/PCA- Details and Data modes

The Proportional Counter Array (PCA) is one of three instruments aboard the Rossi X-ray Timing Explorer[6] and has 5 Xenon gas filled individual units, that detect X-rays in the 2-60 keV range. It is made up of 5 individual units, called the proportional counter units (PCUs), and together comprise a total collecting area of 6500 sq cm. The detectors are made of Xenon gas chambers, arranged in 3 layers (each split into a left and a right), in addition to two veto layers of propane and xenon respectively. Some more specifications forthis device are as follows :
Energy range: 2 - 60 keV (however, the detector is most sensitive in the 3-25 keV range)
Energy resolution: less than 18 percent at 6 keV
Time resolution: 1 microsec
Spatial resolution: collimator with 1°FWHM
Collecting area: 7000 square cm
Sensitivity: 0.1 mCrab
Background: 2 mCrab

The PCA data is sent through the Experiment Data System (EDS), which has six event analysers dedicated to PCA. At this stage, two modes of data are generated, which then go through the telemetry stream. The two principal modes that we will talk about are the event mode and the binned mode.

Event mode data is generated by timestamping each event of detection as it occurs, and labelling it with the PCU and anode layer it was detected at and the 256-channel spectral resolution. For our use, we have used the GoodXenon files, which are generated by two Event Analysers and contain all events that survive background rejection. More specifically, we have only used the GoodXenon files with a telemetry interval of 2s.

The other mode of data available to us is in binned mode, and the science array files we get from this has data binned every few seconds. Most notably,the Standard Product files are in binned mode. However we do not use these as the readout time for the Standard Products was 16s which did not provide adequate temporal resolution, and we can control the time

bin sizes when using the GoodXenon data.

We are also provided with housekeeping files and Filter Files in the original directory, as well as the Orbit Ephemeris for the measurement. However, we have used the Filter Files only for an exercise in how to generate GTI files using the maketime tool, and for our actual data reduction have used the GTI file provided to us in the GoodXenon data files.

Chapter 3

Process of data reduction used

For all our analysis, we have used the High Energy Astrophysics Software created and maintained by NASA's Goddard Space Flight Centre. Our RXTE data is obtained from the HEASARC archives.

We have made use of the FTOOLS package [7, 8] extensively for ourpurposes, as well as the XSPEC module for spectral fitting and estimation of fitting parameters. We will reference several routines from both FTOOLS and XSPEC, and provide citations to the individual recipes where possible.

We have obtained the archival data from the Guest Observer Facility (GOF) archives of RXTE [9] for the proposal id 95354-03-03-00, using the xtemaster table in the Xamin interface. We then proceeded as follows :

3.1 Selecting the data files

We first used the XDF (Xray data finder) tool in HEASOFT to navigate the complex hierarchical directory of the RXTE files obtained from the RXTE-GOF archives, that creates ASCII lists of the group of files as needed and labels them in .xdf format. Using the @filename convention, we can then use these .xdf files in our reduction process. We create separate lists for the GoodXenon (both 1 and 2), Filter Files and the Orbit Ephemeris.

Next, we generated the event FITS file using make_se which combines GoodXenon 1 and 2 into a single eventfile.

3.2 Barycentric correction

Next, we apply barycentric correction to this eventfile. Event files need to be barycentred because the arrival times of photons at the detector are labelled in telescope coordinates. However, the telescope is moving in orbit around the earth, and the earth revolves in orbit around the sun. This gives rise to doppler effects and the arrival times of photons have to be corrected to an inertial frame of reference. The solar system's barycentre is usually taken to be this reference frame.

We do this using the routine faxbary is HEASOFT, which takes the eventfile and the ASCII list of the orbit file we generated using XDF, and appends a column to the event file which gives the barycentric time, and stores this modified copy in a new output event file (alternatively, it can rewrite the original event file but we have chosen not to do that).

3.3 Good Time Intervals

Once the barycentric correction is applied, we need to now select the good time intervals in the entire duration of our data which give us meaningful data to work with. To this end, we must check several criteria to make sure that the data is clean and has the minimum amount of contamination, that we can later correct for using the instrument background and response files. We generate a filter file using xtefilt [10] use the .xfl Filter File given in the Standard Products (found using XDF).

There are several factiors to keep in mind while choosing good time intervals.

3.3.1 Number of PCUs

At any given time, not all the Proportional Counter Units (PCUs) of the RXTE are functional. We plotted the NUM_PCU_ON column to find out how many PCUs were on at any given time throughout the duration of our observation. It is important to note that at the time of our observation, only 2 of the 5 PCUs are on Figure 3.1.

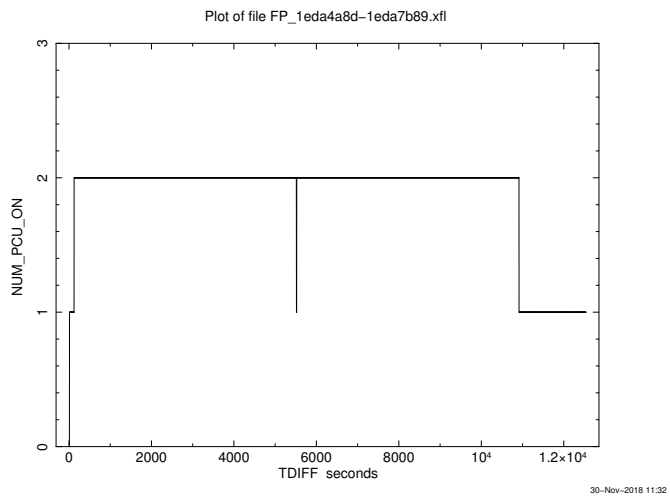

Figure 3.1: Number of PCUs that are recording events throughout the duration of our observation

We also plotted the individual PCUn_ON columns and found that PCU 0 and 1 were off throughout the duration of our observation. This is because of propane loss from both units, which were found to be most likely due to a micrometeorite impact (in May 2000 for PCU 0, and December 2006 for PCU 1) [11]. To further examine the individual PCUs, we have plotted the GoodXenon events for PCU 2, 3 and 4 Figure 3.2.

We can see that only PCU 2 is on for the entire duration of our observation. PCU 3 and 4 are on only partially. This is because in March 1996 some anomalous behavior was noted in these two units and they are only kept on some of the time to reduce further damage.

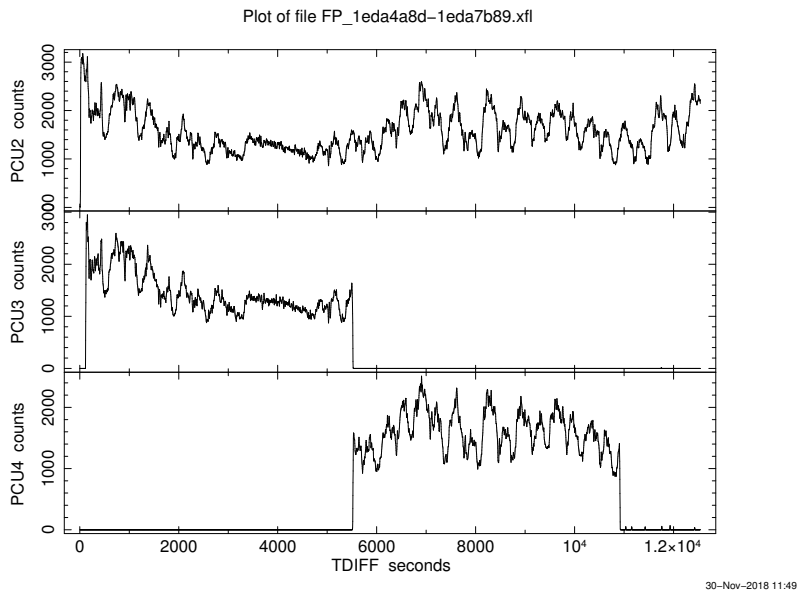

Figure 3.2: GoodXenon events from PCU 2, 3 and 4

3.3.2 Elevation

We plot the ELV column in the .xfl file to check the elevation angle that the target line-of-sight makes with the limb of the Earth, at the spacecraft. This is important because close to limb of the earth, low energy X-ray photons are absorbed by the atmosphere and this distorts the spectrum at those energies. This parameter also provides information about earth occultation, by taking negative values when the source is hidden behind the Earth.

As a general rule of thumb, we discard parts of the observation where the elevation is less than 10°because we want to perform spectral analysis with the data and do not want our it to be from close to the earth's limb. However, as we see in Figure 3.3 the elevation values for our observation are always greater than 17°.

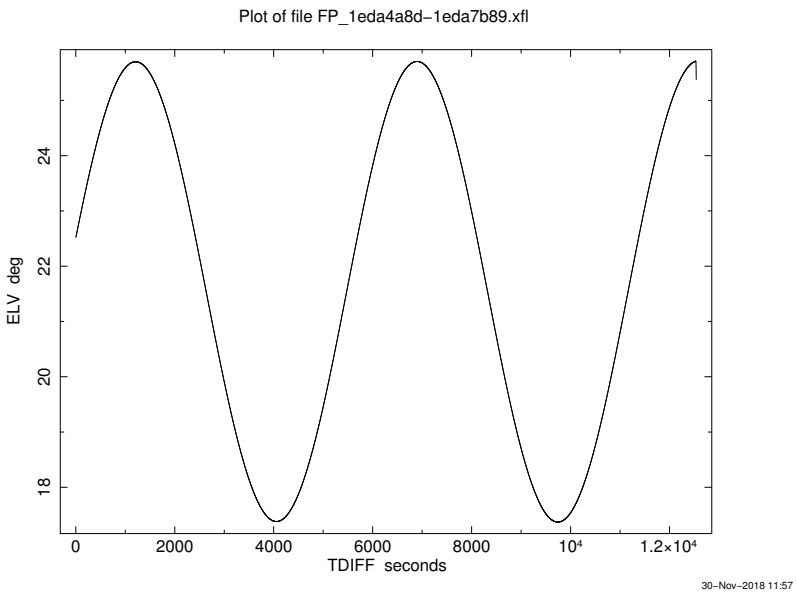

Figure 3.3: Elevation of the target with respect to the Earth's limb

3.3.3 Offset

This column gives us information about the pointing accuracy of the satellite. There is a slight rocking motion of HEXTE which results in the satellite sometimes pointing slightly away from the source, at an angle of about 10^{-3}°. We have plotted this angular offset in Figure 3.4. We usually apply a filtering criterion on the offset to avoid considering the slew that is sometimes present at the beginning or end of the observation. For this purpose, selecting rows where OFFSET$<$ 0.02 is good enough to filter out the slew. From Figure 3.4, it's clear that our dataset doesn't have any slew

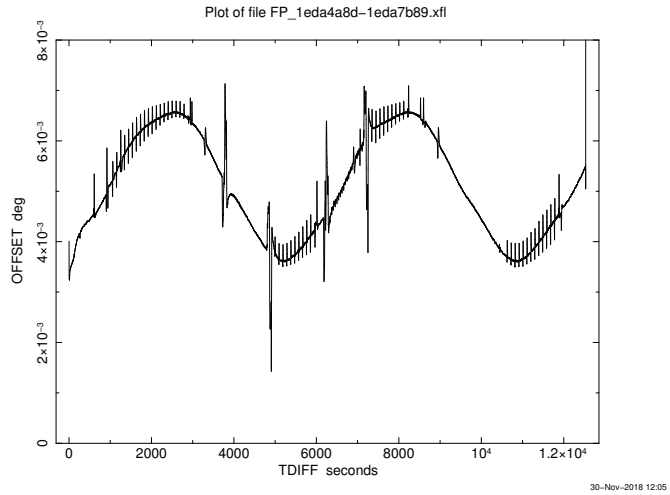

Figure 3.4: Offset in the pointing of the satellite with respect to the target's position

3.3.4 Time since South Atlantic Anomaly

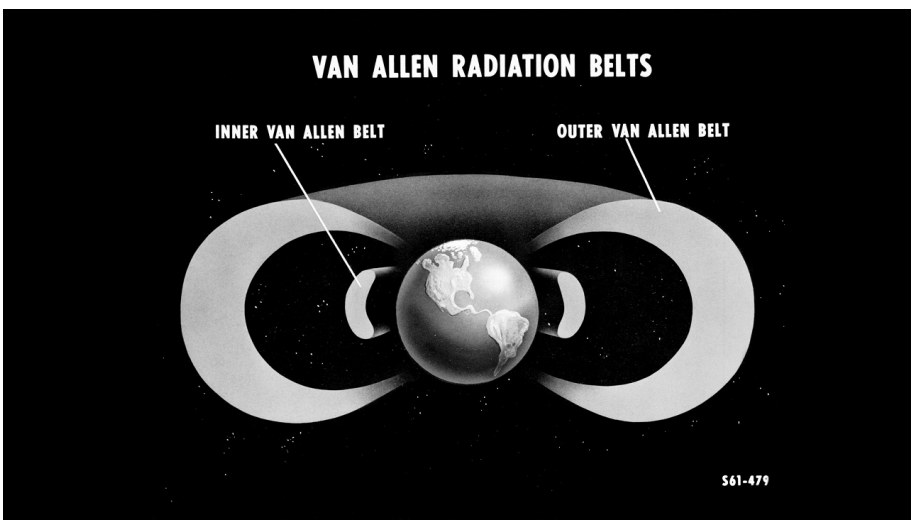

Figure 3.5: The Van Allen Radiation belt
Source : https://www.nasa.gov/feature/goddard/2018/studying-the-van-allen-belts-60-years-after-america-s-first-spacecraft

The earth is surrounded by two concentric zones of energetic charged particles that have been trapped into doughnut-like shapes symmetrically around the earth's magnetic axis by the our planet's magnetic field. This zone is called the Van Allen radiation beltFigure 3.5,

and it lies at a height of about 500-58000 km from the surface. The extent of these belts varies with solar activity as solar winds throw charged particles into the earth's magnetosphere. However, since the radiation belt is symmetric about the earth's magnetic axis and the rotational axis is slightly tilted (at about 11°) with respect to the magnetic, the belt comes as close as 200 km to the earth's surface at its lowest point, over the Atlantic Ocean in the southern hemisphere. This region is called the South Atlantic Anomaly (SAA). Since the belt has highly energetic charged particles, it can bombard detectors and cause damage to them when a satellite passes through the SAA. Close to the SAA, detectors also read out anomalous event counts which are caused by ions and particles in the Van Allen radiation belt, rather than the photons from the source being studied.

We plot the TIME_SINCE_SAA column to see whether there were any SAA passages during our observation. This doesn't always give us the time since the SAA passage as it may seem from its name, but is parameterised to take negative values before SAA, and a steady value of 99.99999 in case of observations where the orbit doesn't have an SAA passage, as we see in our observation Figure 3.7.

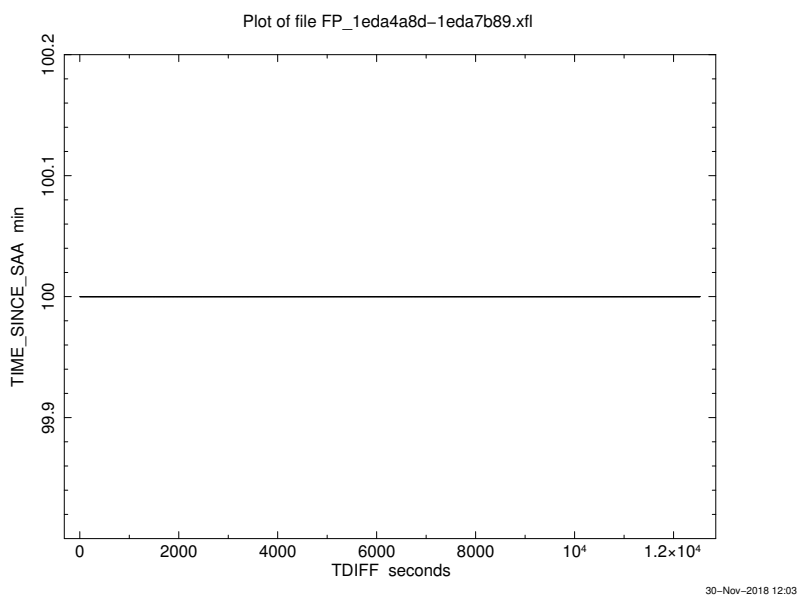

Figure 3.6: Elevation of the target with respect to the Earth's limb

3.3.5 Electron contamination

As discussed in the previous section, energetic particles incident on the PCA cause contamination of event detections. Electrons from solar storms trapped in the earth's magnetosphere, cause an increase in the low energy background. To take care of this, it is recommended to screen observations that have ELECTRON2$<$ 0.1.

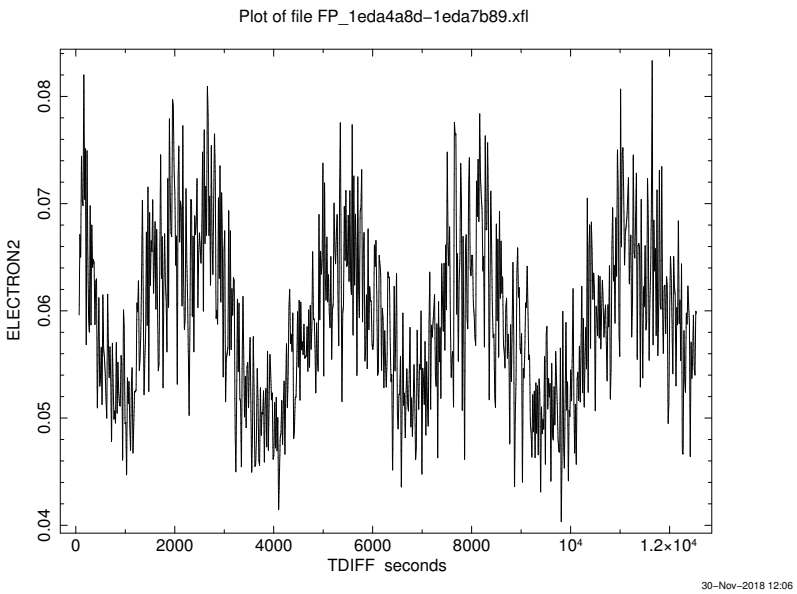

Figure 3.7: Elevation of the target with respect to the Earth's limb

Once we have the parameters for the screening we want to apply,we can extract the GTI file using the maketime tool. However, the GTI file provided by the instrument team with the event file, in the 3rd extension, has some extra hidden screening parameters which are unclear from the recipes provided. Hence we have just used the given GTI extension for all of our analysis. We use the fselect tool from FTOOLS, to apply a GTI filter to our new event file. However, barycentric correction is not applied to the GTI, hence the filtering is done on the original (TT) time column which is retained in the event file. Now we have an event file that is barycentred and has only good time intervals.

3.4 Generating background

We use pcabackest to estimate the background lightcurve and spectra for our event file. We have to do this in a slightly roundabout way. The pcabackest routine takes the Standard2 data files provided to us in the archives, and uses them to generate the background for that interval of time, given the calibration database (CALDB) and model file for that epoch. The latest background is not updated into the CALDB files, so in addition to installing CALDB for our mission, we must also find the pca background model applicable to our epoch and use it for this part.

We obtain the PCA background model for bright sources, for Epoch 5C, which is applicable to our source and epoch of observation (this will be a .mdl file). We also use XDF to obtain the Standard2 event file for our observation. The telemetry interval for Good Xenon files is 2s, but the Standard2 files have time bin sizes of 16s. This may seem like a problem, but the time series analysis of the background light curves has shown that they contain very little power above 0.1 Hz, which effectively translates to the background spectrum being more or less constant within the 16s intervals. For a better background estimation, we would have to do interpolation to apply to data with smaller time bin sizes, which does not work very well according to the instrument team.

We also require the PCA's SAA history file (which can be obtained using XDF). We are using Good Xenon event files, which means that we must expand the estimate of background spectra to 256 channels, and not apply any Xenon gain corrections.

3.5 Generating response

To be able to analyse the spectra from our observation, we must generate the instrument response first. To this end, we use PCARSP, which uses the Calibration Database (CALDB) to generate a .rsp file for each pha file (spectrum). We must obtain the Attitude file using XDF to be input to PCARSP. Even though this is the next logical step for data analysis, in practice we must revisit this steponce we have extracted spectra and lightcurves from our event files and background event files, and generate the appropriate response for each pha file.

3.6 Obtaining the light curves and spectra

Once we have our source and background event files, we can now use them to extract light curves and spectra. We will use the routines saextrct and seextrct for this purpose, saextrct for our source event files and saextrct forthe background files. Since the default time bin size for the background files is 16 s, we will have to further use lcmath to rebin and subtract the background lightcurve from the source. This net lightcurve can then be used for further analysis to find the period of the pulse and to calculate the modulation fraction of individual pulses.

Chapter 4

Analysis

In this section, we will discuss the step-by-step analysis performed with the source and background lightcurves and spectra we have obtained by following the procedures from section 3.6. While doing the analysis, we ran into certain snags and had to redo the analysis several times, so we will also discuss these as we go along.

4.1 Preliminary analysis for the entire observation

In this section we will look at the lightcurve (Figure 4.1) and spectrum for the entire observation as a whole, to find the period of the lightcurve pulses and decide what models to fit to the spectrum.

4.1.1 Fitting a model to the spectrum

We first try to fit a model to the spectrum obtained from the entire observation. We find certain irregularities in the residuals at low energy. This probably happens due to the mismatched response, because from Figure 3.2 we can see that PCU 3 and 4 are not on simultaneously. To fix this, we would have to segregate the part of the observation where PCU 3 is on, from the part where PCU 4 is on. However, this will make the pulse resolved spectroscopy difficult for different parts of the observation, because it will hinder the com-

parison of parameters from different pulses if the detectors aren't uniform across the board.

To eliminate this complexity, we will create a bitmask [12] that selects only the events from PCU 2. This unit has the highest throughput, and has functioned most consistently over the lifetime of the RXTE, hence this is a prudent choice for our analysis. We generate a new response file to correspond to this choice, and use this response file for all further analysis, because the response file doesn't change on the timescale of our observation.

For fitting the spectrum, we will try to replicate the results from Gogus et al. [4]. We use the energies from 3-25 keV for fitting, because this is where the detector is most sensitive and will help us compare the different parameters of the pulses as they evolve over the observation. At first, we use a basic power law to fit the pulse, with a photon absorption component for the lower energy, and a Gaussian for the iron line at 6.4 keV. As we will see in our later fits, we will run into some problems with the Fe lines that we will discuss as we go. We also try the cutoff power law and the broken power law instead of a normal power law.

4.1.2 Finding the pulse period

To obtain the pulse period of our lightcurve, we first try to use powspec which generates a power spectrum (Figure 4.1) from a time series, in our case a lightcurve. By inspecting this power spectrum, we can see two prominent peaks at around 0.0015 Hz and 0.003 Hz. This is expected, because each pulse has 2 peaks roughly (Figure 4.1).

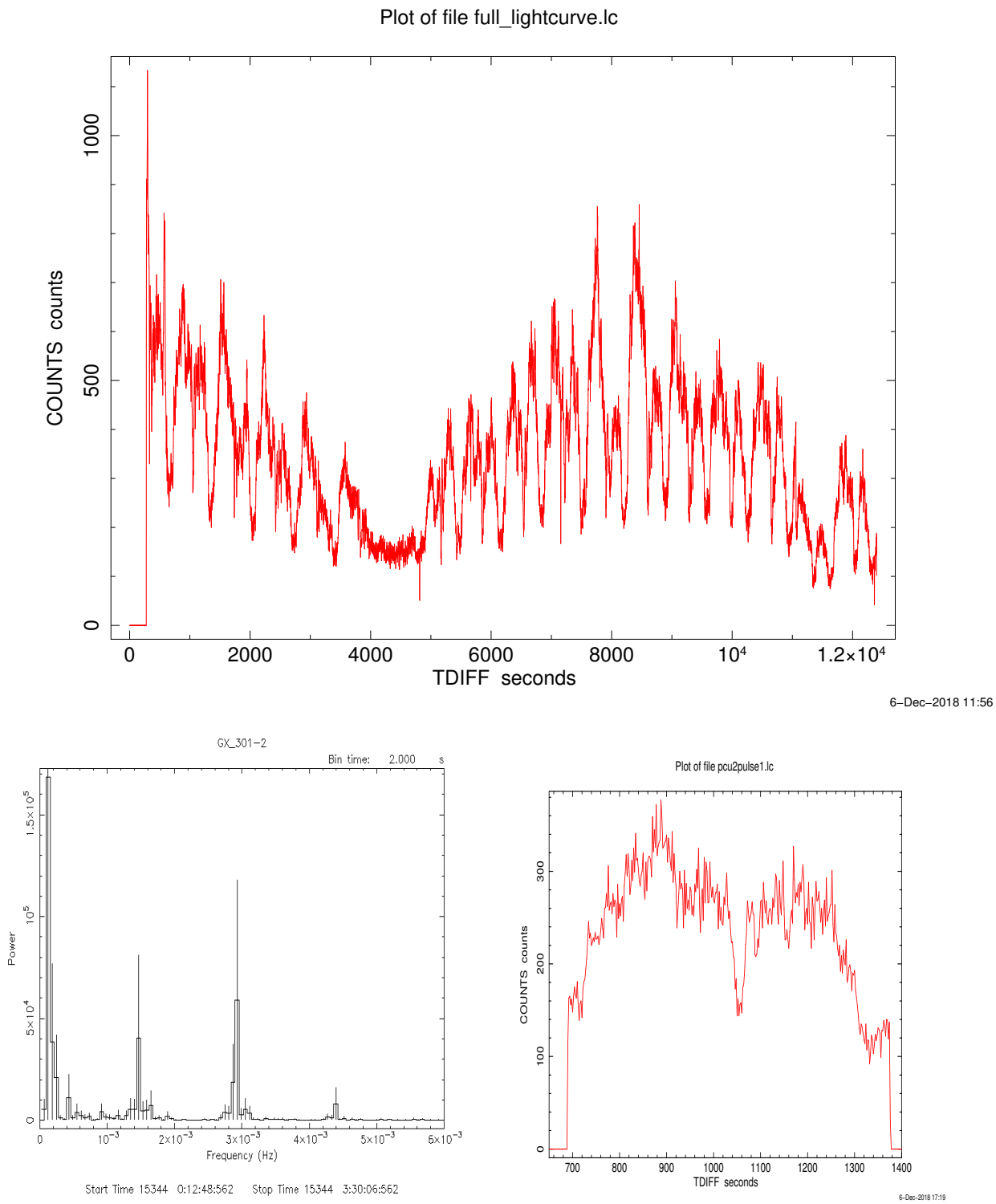

Figure 4.1: Top panel: The complete lightcurve of our observation, with the dip visible just after 4000 s
Bottom Left panel : the power spectrum given to us by powspec. We can distinctly see two peaks, one close to 0.0015 Hz, and the other around 0.003 Hz.
Bottom Right panel : A solitary pulse, which shows the double-peaked structure.

Since we want to find the period of the entire pulse, we will take the lower value of the two harmonics, which comes out to be around 0.00147(1) Hz. This gives us a period of around 680 s, which will be the starting point of our search for the pulse period using efsearch.

However, we run into some problems with efsearch. The search gives us a chi square profile that has peaks and dips, that sit on a larger continuum of a profile that resembles a Gaussian Figure 4.2. This may be because of the way efsearch finds these peaks by folding the light curve with different period sizes. Since the lightcurve is quite variable in the vicinity of the dip, this may be giving rise to such fluctuations in the efsearch chi square parameter.

To check whether the period given by efsearch is close to the actual period or not, we must fold the lightcurve using efold. We give it different period values, like 680 s, 683.85 s (the best fit value from efsearch), 686 s (from literature[1]) and see which lightcurve looks the least smeared. We settle on 686 s, as this has the least smear and agrees with the literature value.**??**

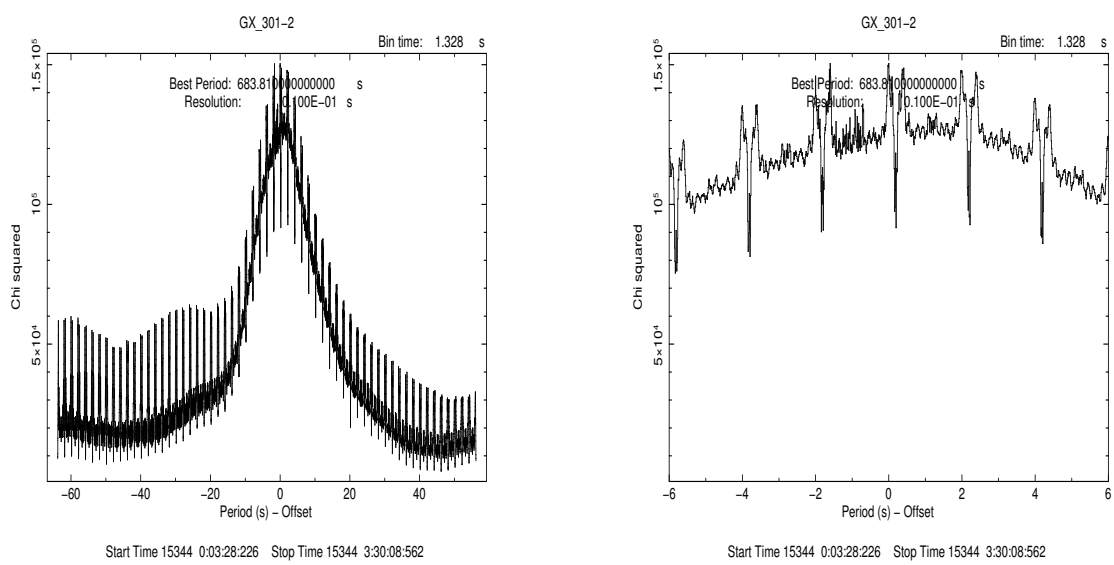

Figure 4.2: Left panel : the continuum in efsearch results
Right panel : The variation on a finer scale.

4.2 Analysing each pulse

To examine what is going on in the system before, during and after the dip, we must isolate each pulse and look at it separately. For this we will use the method of phase calculation to separate the observation-long lightcurve into its individual pulses. Phase is given by :
$\phi = \nu(t - t_0) + \frac{1}{2}\dot{\nu}(t - t_0)^2 + \frac{1}{6}\ddot{\nu}(t - t_0)^3$
where t_0 is the first time value in our observation
$\nu, \dot{\nu}$ and $\ddot{\nu}$ are the frequency, and the first and second derivative of the frequency respectively.

By examination of our lightcurve, we find the start and end phase of each pulse and segregate the first 14 pulses.

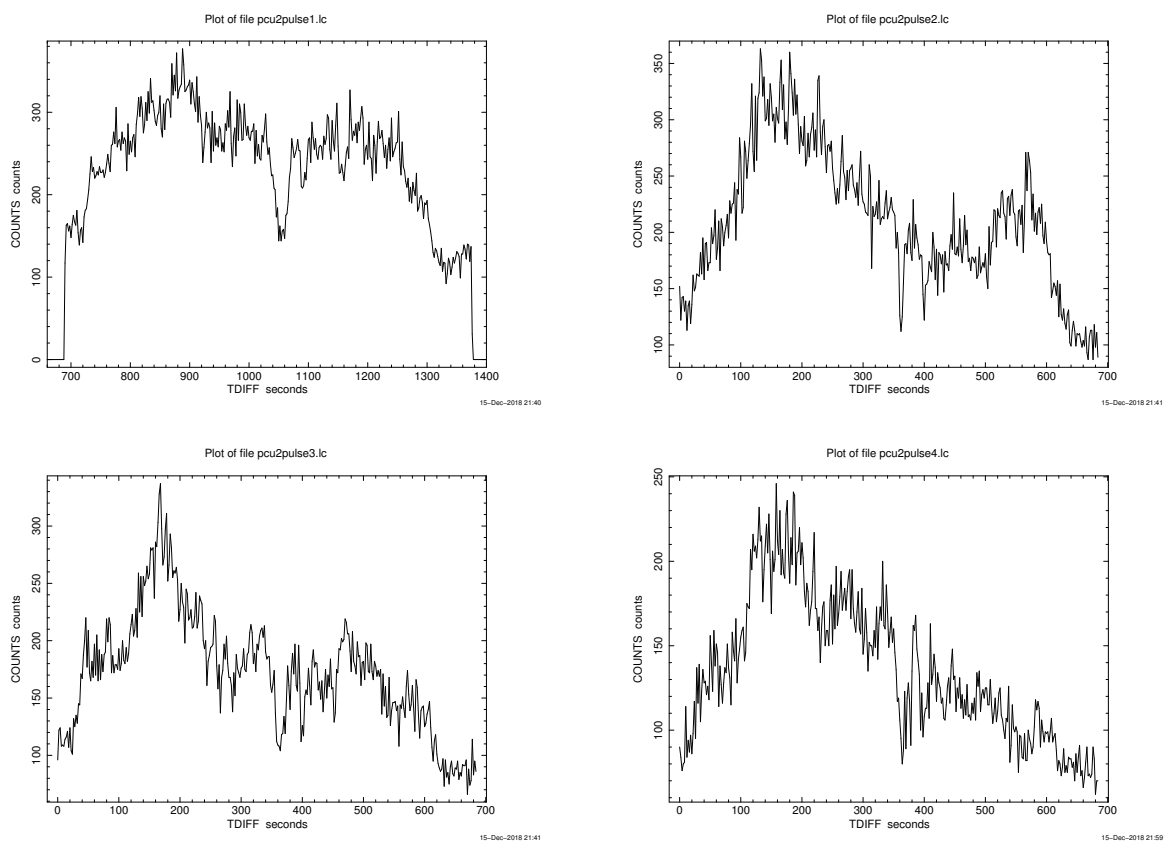

Figure 4.3: Pulses 1, 2,3 and 4

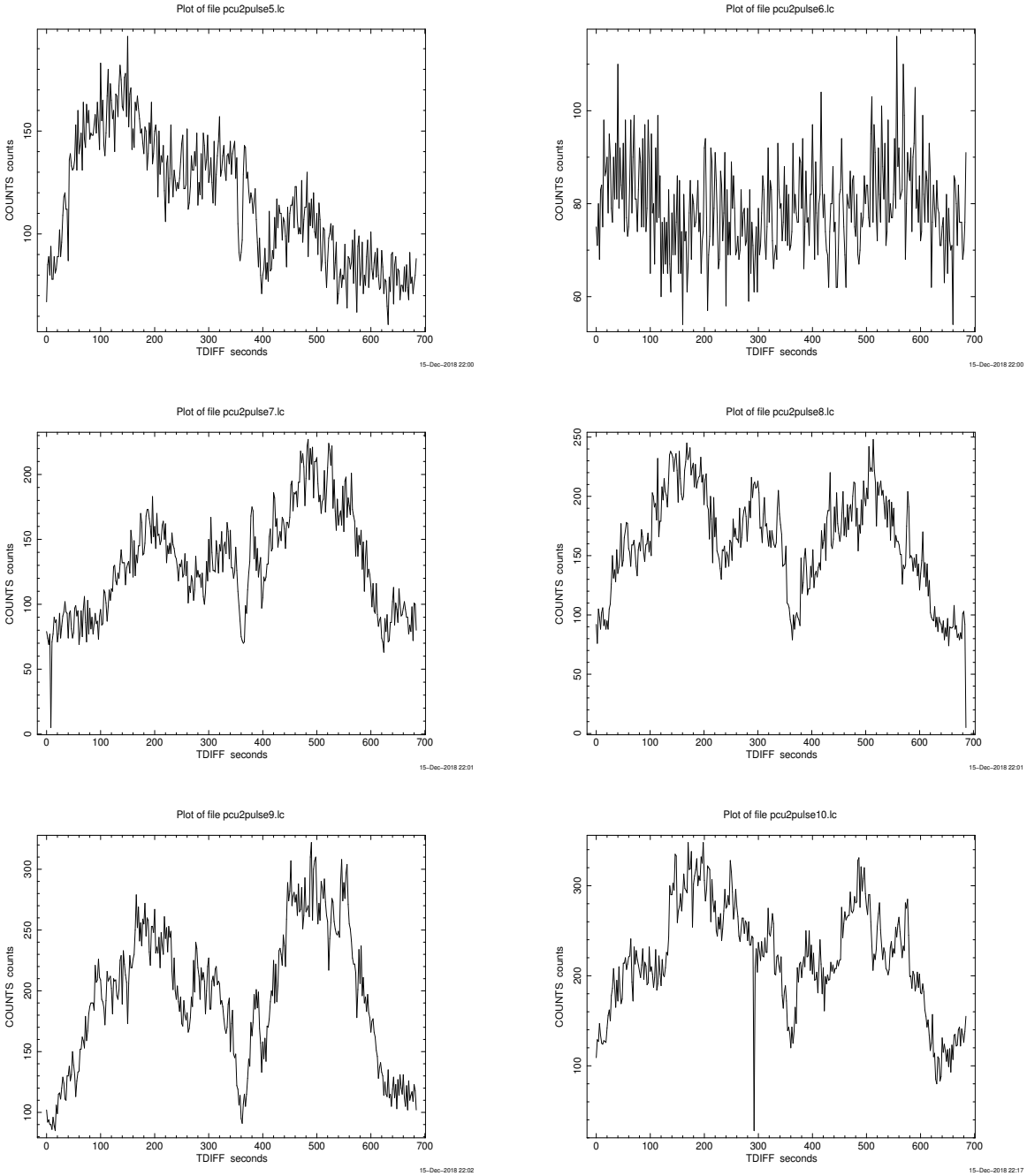

Figure 4.4: Pulses 5, 6, 7,8, 9 and 10. Pulse 6 is clearly where the dip occurs

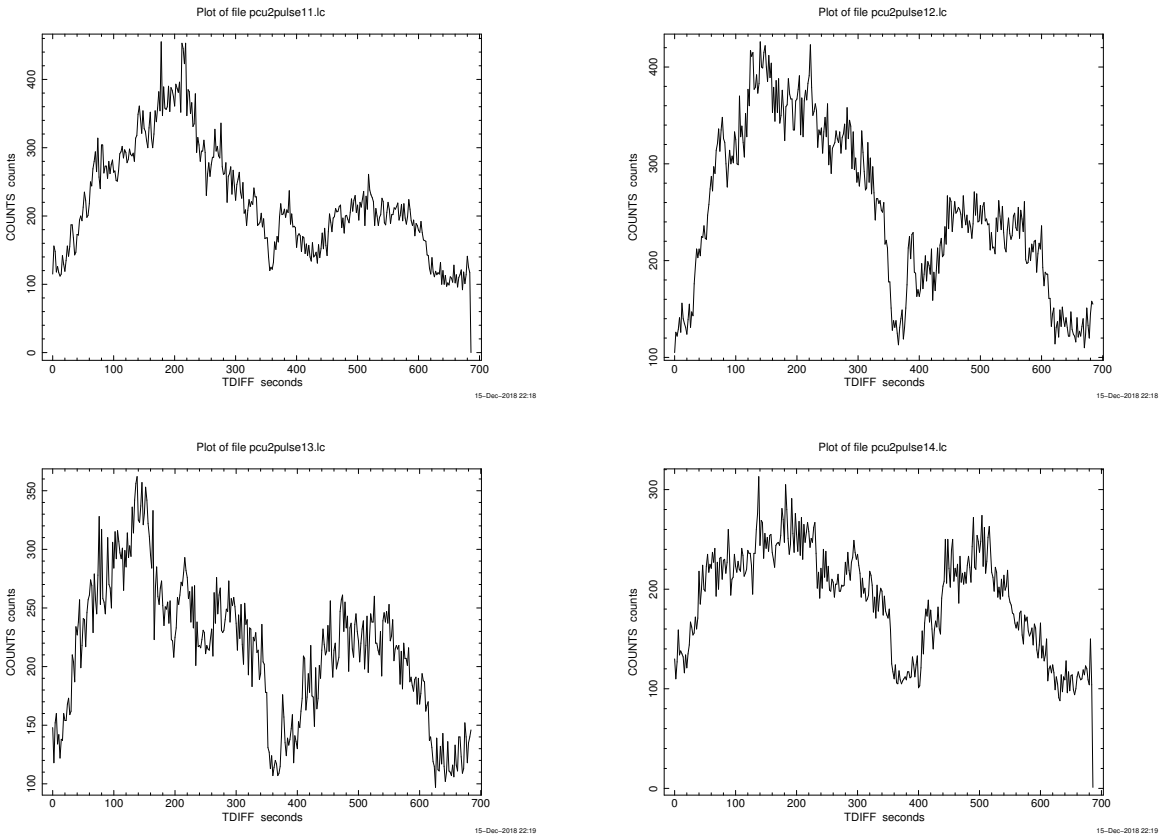

Figure 4.5: Pulses 11, 12, 13 and 14

Right at the outset, we run into trouble because the counts are too low once the background is loaded. This, as it turns out, happens because the Exposure time label in the header of the pha files, is not corrected when we use fselect to separate the pulses. Henceforth, we always make sure to correct Tstart and Tstop by hand before extracting lightcurves and spectra from the individual fits files of the pulses.

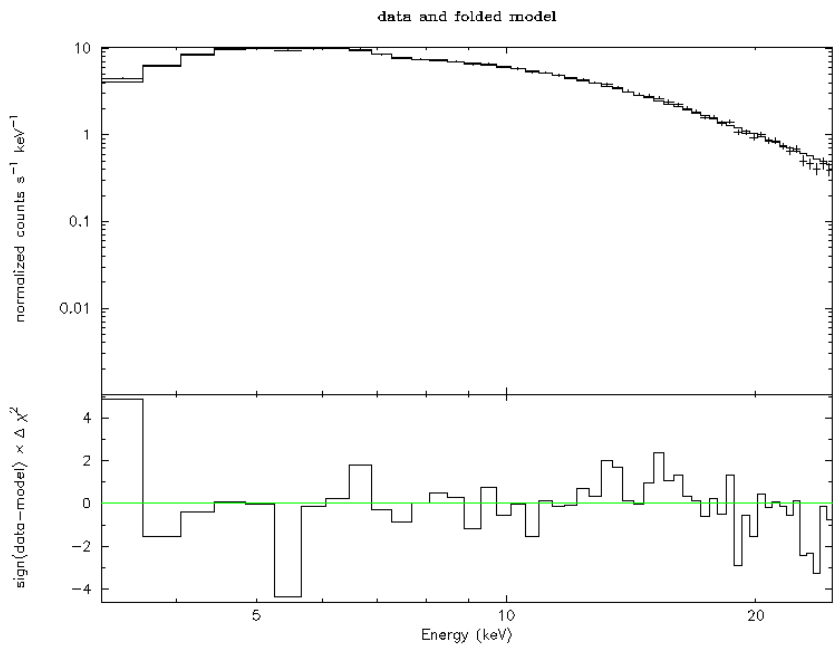

Figure 4.6: A sample fit for the 1st pulse

Figure 4.7 shows a sample fit we do to the first pulse. We have used an absorbed power law to describe the spectrum, and a Gaussian at 6.4 keV to represent the Fe line. We fit in the 3-25 keV range because this is where the detector is most sensitive. Right off the bat we can see a weird wiggle shape near 5 keV. From RXTE FAQs,we found that this is the Xenon L-edge that appears at 4.8 keV. We fix this by using a systematic error of 2%. We can see that this improves the fit and the chi square:

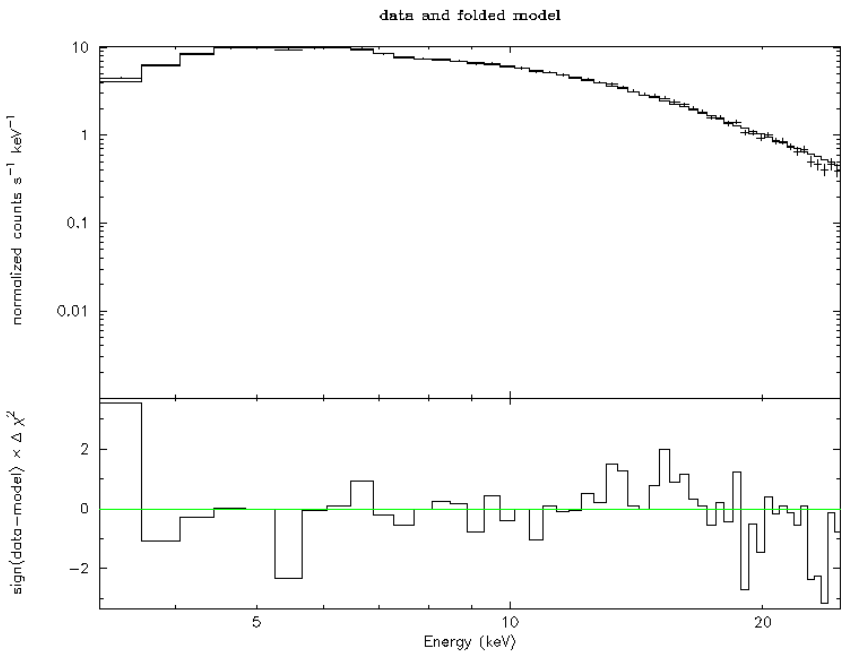

Figure 4.7: A sample fit for the 1st pulse, with systematic error added

In this section, we tried multiple models such as cutoff powerlaw and broken powerlaw as well. Cutoff powerlaw did not work in this case because the folding energy for this object is around 30 keV, where the signal to noise ratio is poor. As a result, we had to settle for broken power law or power law, both of which gave comparable fits once the systematic error was set to 0.02. There are some pesky residuals at lower energies which continue to be there despite our best efforts. This may be due to a response problem at low energy, or a large absorbed component at the lower energy. This is somewhat fixed by using broken power law instead of power law for the fit, but not very radically. For the sake of simplicity, we used the powerlaw. And we have plotted the results of our spectral analysis for all the pulses.

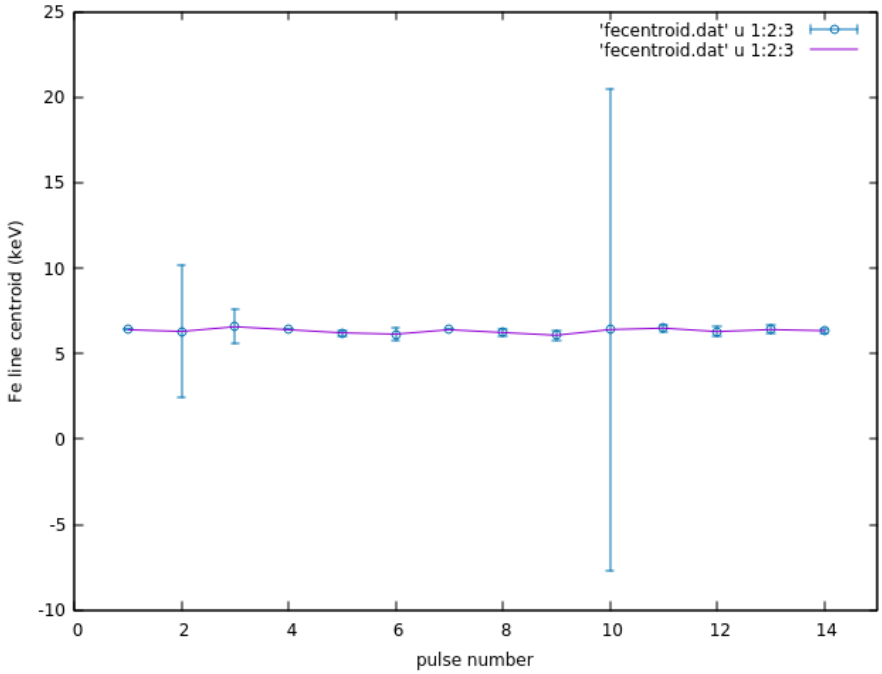

Figure 4.8: The iron line centroid

We can see that the iron line centroid has a slight problem. This is because the Fe line is not well constrained and gives trouble when we try to fit it. For our purposes, we have fixed the energy of the iron line.

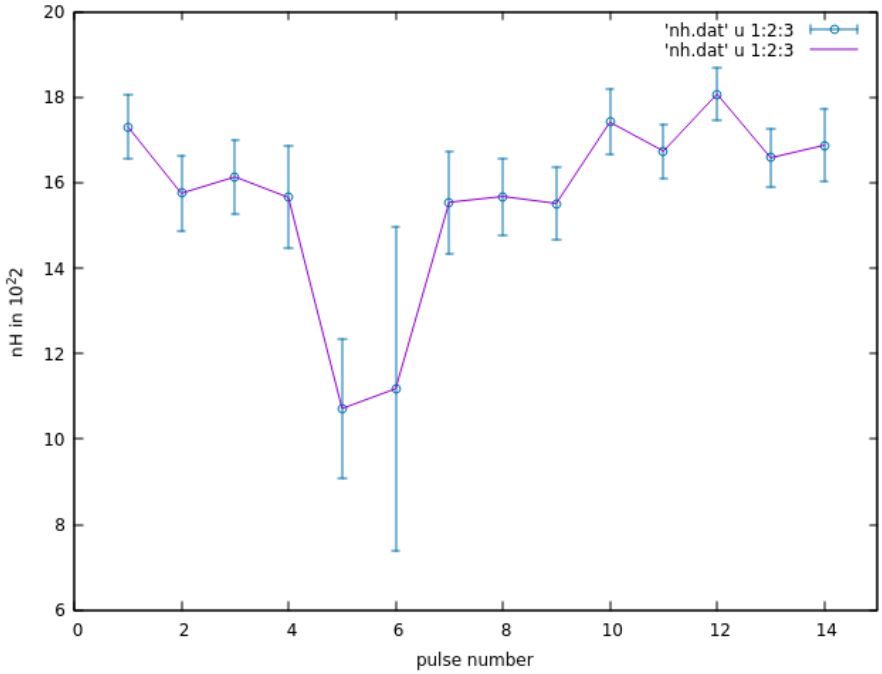

Figure 4.9: The hydrogen column depth

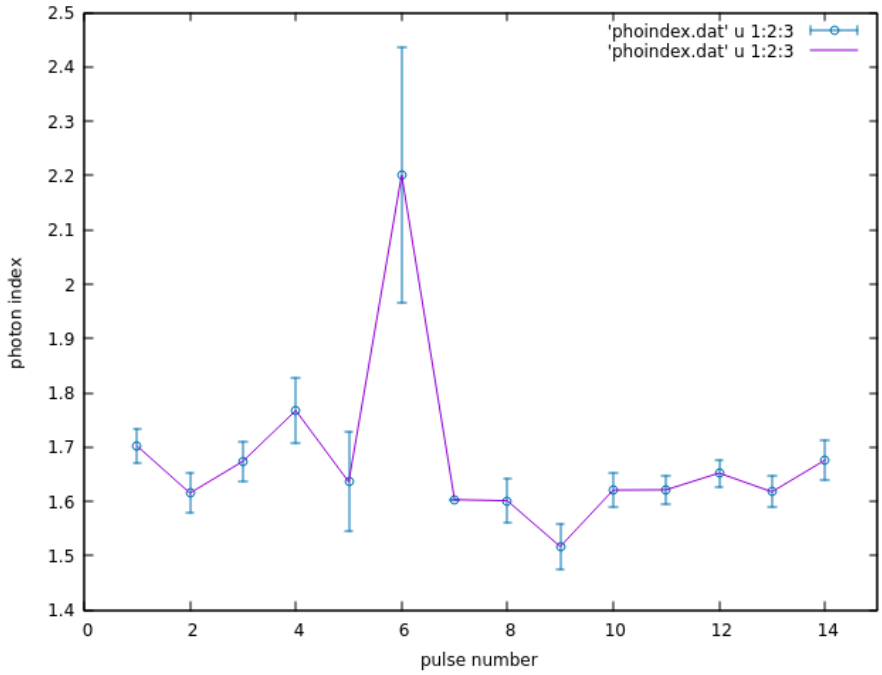

Figure 4.10: The photon index

We can see how the Hydrogen column depth reduces near the dip, and the photon index (which gives the negative slope of the logarithm of the spectrum) rises. We will discuss these interesting results in the discussion section. To check if there is a pulsed component in the dip,we calculate the modulation fraction of each pulse.

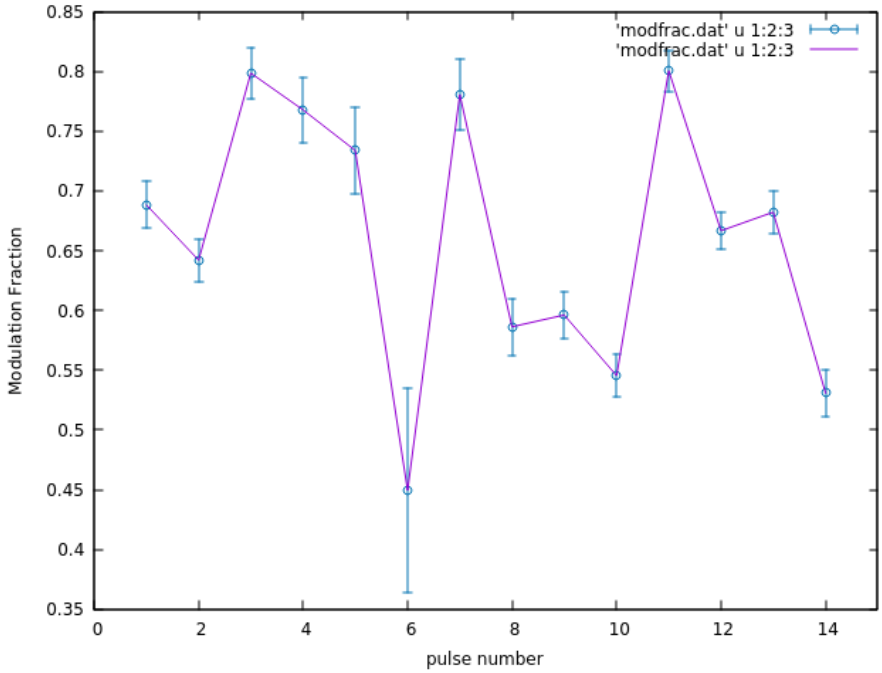

Figure 4.11: Modulation fraction

The modulation fraction is a quantitative way of measuring whether a set of data contains a modulated signal or a bunch of random data points that are akin to background noise. For a perfectly modulated pulse, the modulation fraction is 1. For a random unmodulated signal, the value of this parameter should be vanishingly close to 0. However, we see that this modulation fraction is nowhere close to 0 for the dip, it is nearly 0.45(10). This means that there is a residual pulsed component present even at the minima, and the pulse never really disappears. This is more prominent when we take larger time bin sizes to bin our lightcurve, as shown below.

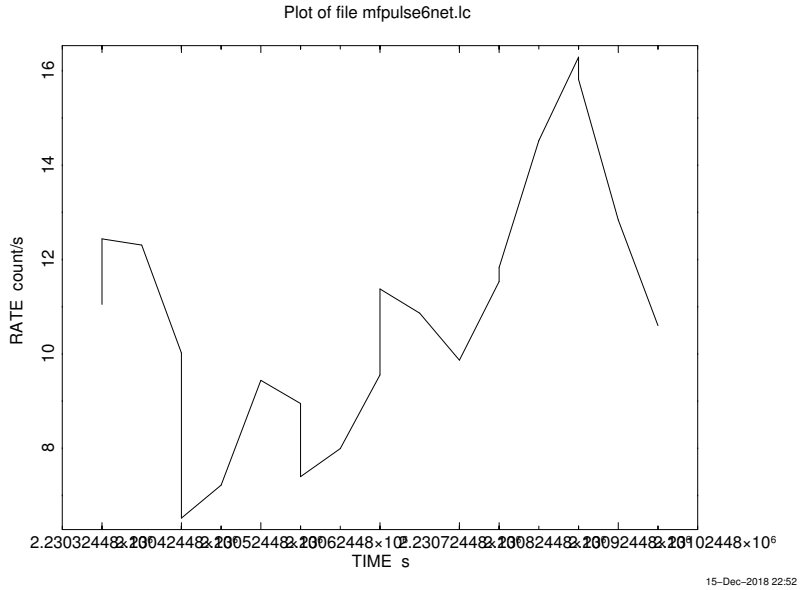

Figure 4.12: The 6th pulse, with 16 s bins, shows some semblance of a pulse shape

4.3 Analysing component pulses before and after the dip

To compare the spectral characteristics of the primary and trailing pulse, we must analyse them separately. To this end, we have binned the primary pulse for all pulses below the dip, and also for all pulses after the dip. We did the same for the trailing pulse. So the pulse1 is the pre-dip primary pulse, pulse2 is pre-dip trailing pulse, pulse3 is the post dip primary pulse and pulse4 is the post dip trailing pulse. We use fselect to create these files. However, it is not trivial to process them because we must create a GTI file that reflects which parts of the data we have taken. We can do this using the maketime tool by giving it the same filtering values we input to fselect. We then use mgtime to merge the existing GTI and our new GTI so that we eliminate the bad time intervals in our data. We use this new GTI file in saextrct and seextrct as the GTI OR file. We must also remember to correct the Tstart and Tstop in each fits file so that the exposure is calculated correctly (it takes the GTI into account automatically while extracting the light curves and spectra).

For some reason, it is especially difficult to fit an absorbed power law to these spectra. We resort to using bknpower and fixing the position of the Fe line. The break energy is more or less consistent within all the 4 pulses.

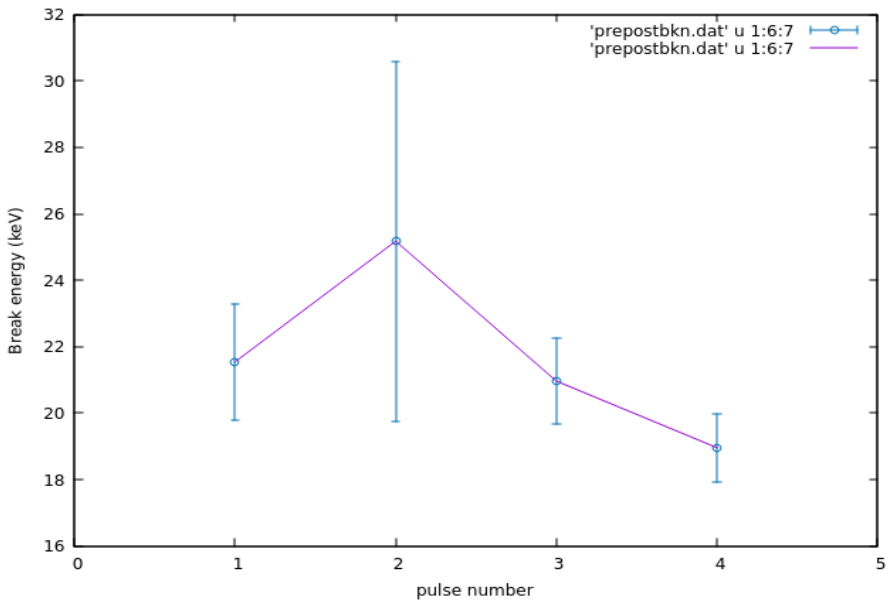

Figure 4.13: Break energy for all the fits

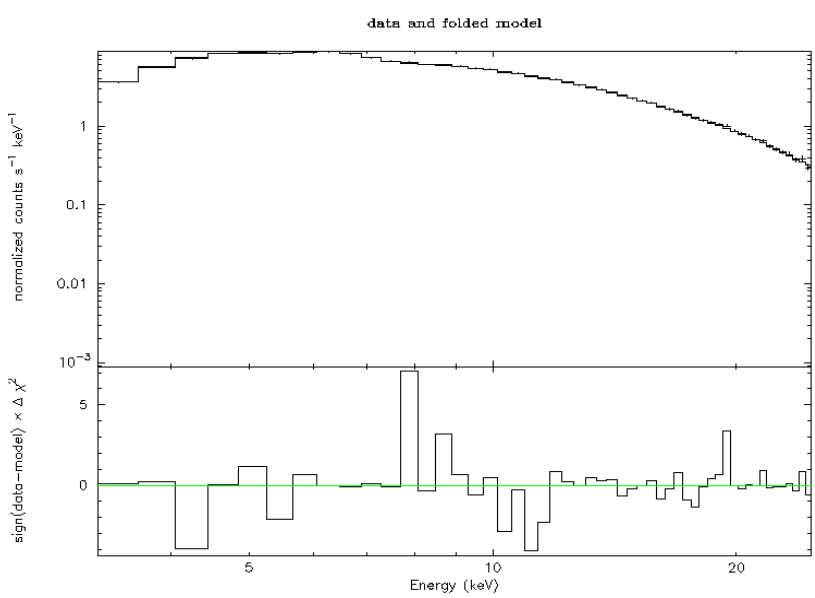

Figure 4.14: A sample fit using broken power law : the primary pulse post dip. There are some stray points with a higher chi square, but there is no trend or pattern in the residuals.

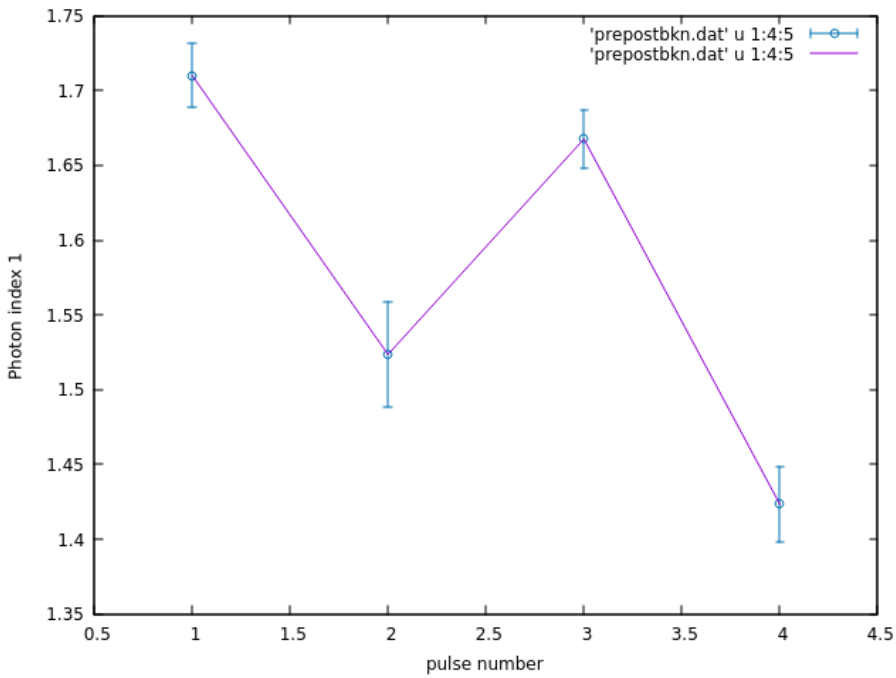

Figure 4.15: Photon index 1

The primary pulses (1 and 3) before and after the dip have consistent photon indices, and are more than 3σ away from the photon indices of the trailing pulses (2 and 4) which lie within about 1σ of each other. This shows that the primary pulse originates at a different geometric location than the trailing pulse, quite possibly an opposite pole.

Chapter 5

Discussion

From our analysis, we can see how the pulse characteristics change as it comes close to the dip and then goes away from it. It must be noted that the pulse never completely disappears, but some part of it is still discernible in the 6th pulse (where the dip occurs), even though the counts fall sharply. The modulation fraction is a quantitative way of measuring whether the pulse shape has completely disappeared or not, and we see that the fraction never goes below 0.3. Let us go through the various possible reasons for the occurrence of the dip, and try to eliminate as many as we can.

5.1 Previously discussed phenomena

Göğüş et al. [4] put forward, and refuted, some possible reasons for the dip. Let us take a look at them.

5.1.1 Absorption by interstellar gas clouds

Wherever dips in pulses such as ours are observed, absorption is the first phenomenon considered for a change in the lightcurve. As expected for such an effect, the counts in the lightcurve go down for our observation as well. However, it is observed that the pulse also gets softened (as we can see from the photon index increasing in value, which means it

becomes more negative and hence denotes a softening of the spectrum). If there was absorption occurring, the softer (less energetic) photons would be more likely to get absorbed or scattered. As a result, there would have been an overall hardening of the pulse, which is not observed. Moreover, we can see from the plot of nH, that the hydrogen column depth has also decreased, contrary to what we would observe if there was an occluding cloud that was absorbing the photons.

5.1.2 Propeller effect

Sometimes, following a burst of X-ray intensity from an accreting pulsar, the X-ray pulses seem to disappear for a period of time. During this time, the pulse may completely disappear, or a remnant of radiation from the surface of the neutron star may become visible in the absense of the much brighter jet. This happens when the magnetosphere of the NS briefly propels out the accreting matter, and accretion ceases for a brief period following a burst of heightened accretion due to a Roche lobe overflow of the companion or a sudden burst of stellar wind. Some people believe that this could explain the dip [13][14][15]

We define the propeller regime as the situation when the radius of corotation of the accretion disc becomes smaller than the Alfven radius for the magnetosphere. This implies that the plasma couples with the magnetic field and is ejected out from the poles.

In the case of our object, we calculate the model flux from XSPEC for the 3-25 keV band, and use this to find the mass accretion rate at the time when the first pulse is observed. This comes out to be approximately $1.4 * 10^{-10} M_{\odot} yr^{-1}$. Using this, we compute the Alfven radius, which comes out to be $25,983$km. Using the spin period of the neutron star and its mass taken to be $1.4 M_{\odot}$, we calculate the corotation radius. The value of this according to our calculation is about $1.3 * 10^5$ km. Our corotation radius is greater than the Alfven radius by an entire order of magnitude. The variation in the flux for our observation can only change the Alfven radius by a factor of 1.9 at maximum. This proves that the object will never really go to the propeller regime, hence the propeller effect cannot be a reason for the dip in the pulse.

5.1.3 Brief stop in accretion flow

Some literature on this topic also theorizes that the dip maybe due to a brief cessation in the accretion flow [16][17].

Using our value of mass accretion rate from earlier, we have computed the viscous timescale of our object, given by

$$t_{\mathrm{visc}} \sim 3 \times 10^{5} \alpha^{-4/5} \dot{M}_{16}^{-3/10} M_{\mathrm{bh}}^{1/4} R_{10}^{5/4} \quad \mathrm{s}$$

Figure 5.1: Viscous timescale. source : [18]

In our case, the accretion disc parameter of viscosity α is not an empirical value. It is an unknown constant that varies with the system behaviour. If α is taken to very small values of about 10^{-2}, the viscous timescale approaches values of about 400s, which is close to the period of our NS (686 s). What this could possibly mean, is that the inner disc modulates the accretion close to the surface and for some reason, this accretion may be reduced to a diffuse flow for a brief period due to the variability of the inner disc. This would explain the gradual fall and recovery of the luminosity, as well as the presence of the pulsed component in the dip since the accretion rate is only lowered, never stopped completely. This makes sense, since the accretion rate must be as low as $4.95 * 10^{-13} M_{\odot} yr^{-1}$ for an onset of total cessation of accretion, and all our mass accretion rates are 3 orders of magnitude higher than this value.

5.2 Our hypotheses

In this part, we discuss some hypotheses that were not discussed by Göğüş et al. [4], and whether or not these are viable, given the results of our analysis.

5.2.1 Occlusion by opaque object

The pulse obscuration happens in stages, the primary pulse becomes less luminous and then the trailing pulse follows, until the dip when the trailing pulse becomes slightly more prominent than the primary and re-emerges from the dip with that characteristic, and then goes back to its initial shape after 5 or 6 pulses. Some have theorised for other objects, that this may be due to an asteroid or similar opaque matter passing through the field of view and obscuring the system [19]. Some also claim that this may be due to the variability or clumpiness of the wind that is emitted from Wray 977 [13][20].

However, on close inspection of the primary and trailing pulse before and after the dip, we can clearly note that the spectral index of the either pulse remains even after the dip. The similarity in spectral characteristics within the primary pulse, and its distinct difference from that of the trailing pulse, points to the conclusion that each pulse originates at a geometrically different region of the NS. Possibly, the two poles.

For the pulse shape to gradually change and reappear, there would have to be a co-moving clump of matter at the origin of the beam, since the effects of its movement persist beyond a single pulse period in a gradual but similar fashion. Since the gradual change is observed in both pulses, there would have to be a co-moving mass at each pole, to observe the gradual fall in luminosity as it occludes each beam, and then the reappearance of the pulse as it moves away. While this is a valid scenario, it seems highly implausible to have two co-moving masses at each pole at the same time, behaving in the same manner.

5.2.2 Magneto-hydrodynamic instability

In a seminal paper, Romanova et al [21] showed through simulations that magnetohydrodynamic perturbations in rotating, accreting neutron stars could cause instabilities that cause a drop in the luminosity of the pulsar. This was a direct result of the accreting matter penetrating the magnetosphere of the NS, forming smaller funnels of accretion rather than two main funnels at the poles. As a result, the polar accretion would temporarily go down and the pulse luminosity would decrease drastically.

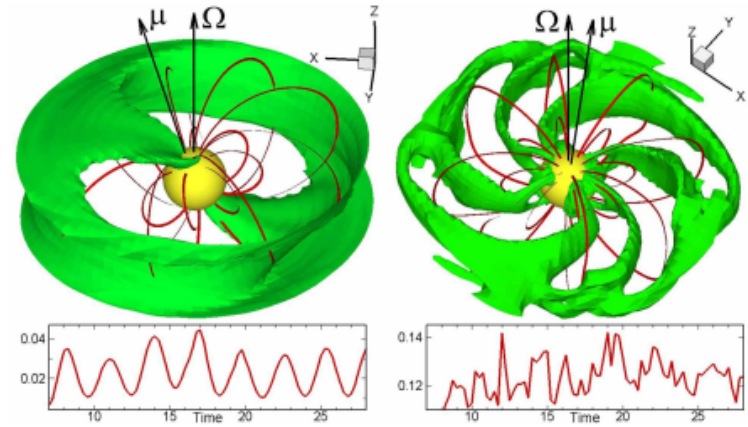

Figure 2. *Left:*Accretion in stable regime. The surface is a constant density surface, and the lines are sample magnetic field lines. The magnetic axis of the dipole μ is inclined relative to the rotational axis Ω at $\Theta = 15°$. *Right:* Accretion in the unstable regime at $\Theta = 5°$ (from Romanova, Kulkarni & Lovelace 2008).

Figure 5.2: Magnetohydrodynamic instability. source : [21]

However, the critical mass accretion rate for a neutron star for such a phenomenon to occur, is given by the formula :

$$\text{NSs}: \quad \dot{M}_*^{\text{cr}} \approx 2.2 \times 10^{-9} (B_*/10^9\text{G})^2 r^{\frac{5}{2}} m^{-\frac{1}{2}} M_\odot/\text{yr}.$$

The period in dimensional units is:

$$P_* = A_p P_*^{\text{dim}} m^{-\frac{1}{2}} r^{\frac{3}{2}},$$

where scaling factors for different stars are:
CTTSs: $A_p \approx 1.78$ days, $r = R_*/2R_\odot$, $m = M_*/0.8M_\odot$,
WDs: $A_p \approx 29.4$ sec, $r = R_*/5 \times 10^8$ cm, $m = M_*/1M_\odot$,
NSs: $A_p \approx 2.22$ ms, $r = R_*/10^6$ cm, $m = M_*/1.4M_\odot$.

Figure 5.3: Critical mass accretion rate for MHD instability source : [22]

Going by this formula, the critical rate of accretion for our object would be $3.52 * 10^{-2} M_\odot yr^{-1}$,which is several orders of magnitude higher than the accretion rate for our system. What this means, is that the accretion rate in our system never overwhelms the magnetic field strength to pass over into the unstable regime. Hence, even though small

pockets of such instability may occur, it is highly unlikely that it ever overshadows the periodic nature of the pulse, and is always much less prominent than the accretion column's luminosity.

5.2.3 Geometry of the beam

We observe the pulsar when our line of sight cuts through the beam of the NS emanating from its poles. If due to some reason (like a hydrodynamic instability in the wind, like a shock front at the accretion column [20]) the geometry of the beam with respect to our line of sight changes, we could see an effect resembling this dip.

Either the beam geometry could be changing (for example from a pencil beam to a fan beam), such that the line of sight cutting through the beam picks up only a part of it, then the light curve would look exactly as it does in our case, with a decline and then rejuvenation of the luminosity. This would also happen at both poles, hence we would see different parts of the beam at each pole, giving rise to the relative changes in pulse shape.

Alternatively, if the beam were precessing, we would observe a dip when the beam mostly disappears from our line of sight. This would also explain the short time frame of the dip. Since the line of sight cuts through a different section of the beam at both poles, we would observe a relative difference in the luminosities of each pulse. This also aligns with the gradual drop and recovery of the pulse luminosity before and after the dip. However, this would mean that the precession would be periodic and the dip would re occur after a certain period of time. The problem with this is that large observation times with one object with a good enough resolution to observe the dip, are not trivial to isolate and examine, unless we are specifically searching for it. So far, such a dip has not been reported for GX 301-2 at any other instance.

Chapter 6

Conclusion

To summarize the above chapters, we have eliminated the following candidates for the cause of the dip : absorption by gaseous matter, occlusion due to clumps of matter, propeller effect and MHD instability (a la Romanova et al.[22]).

Through the spectral and timing studies and calculation of time scales, the following candidates are still in the running for plausible causes : brief reduction in accretion due to temporal shifts in the inner disc, precession of the neutron star,or a brief change in the geometry of the beam. At this point, these three are indistinguishable as far as our analysis goes.

We will be doing further calculations to estimate the timescale of precession and the torques necessary for it, and then try to predict the re-occurrence of such a dip and look for it in Astrosat or RXTE data having long exposures. We will also check the other regimes of instability like the Kelvin Helmholtz instability[23], hydrodynamic shock formation in the accretion column [20], and others, and the timescale at which they operate to see if they could be ruled out as possible candidates. We will also try to study in detail whether a transition between Compton and radiative cooling near the accretion column could be at play here. Hopefully, we will be able to rule out most of these and be finally left with just one explanation, so as to be able to definitively explain the reason why such a dip occurs.

Chapter 7

Appendix : A

Let us walk through the analysis process I have used for Crab pulsar usingLAXPC data, and try to understand how it is done, as well as some technical details.

7.1 The Detectors on Astrosat

There are 3 detectors on board the Astrosat that are relevant to us : SXT (which operates at 0.3-8 keV), LAXPC (3-100 keV) and CZTI (10-150 keV).

LAXPC or the Large Area Xray Proportional Counter, is an array of 3 co-aligned x-ray photon counters that are used to do timing studies and low resolution spectral studies. It has a field of view of 1deg x 1deg (to minimise source confusion), and is built to achieve high detection efficiency over a large energy band, with small internal background and moderate energy resolution. (summarised from IUCAA's Astrosat website) At present, 2 of the 3 LAXPC counters, namely LAXPC 10 and LAXPC 30, have run into problems involving gas leakage and anode wire malfunction.

The Cadmium Zinc Telluride Imager (CZTI) is a hard X-ray imaging device, whereas the SXT is Astrosat's Soft X-ray Telescope. I have done analysis with some data from LAXPC,

for the purpose of this project.

7.2 The Object : Crab

As mentioned in the abstract, the primary objects of interest for the project are Cygnus X-1, GRS 1915+105 and GX 301-2. But to learn the techniques of timing analysis, I have started working with LAXPC data of the Crab pulsar.

The Crab pulsar is a neutron star pulsar in the supernova remnant Crab Nebula. It is a very popular calibrating source in X-ray astronomy, and has a period of roughly 33 ms. Since it is a fast pulsar with a sharp, strong signal, it can provide arrival times very accurately. We will talk about the source more as we analyse it.

7.3 Step 1 : Pipeline

The level 1 data, after the first step of cleaning, has to be parsed into a useful form for us to be able to analyse it. For this, all 3 of our detectors have dedicated pipelines. For our use for LAXPC data,we have used Dr Ranjeev Misra's (IUCAA) pipeline to extract spectra and lightcurves from our level1 data file. The level1 files are taken as input by the pipeline to generate eventfiles and filterfiles, which then give us the FITS event file and the FITS good time interval (GTI) files respectively.

7.4 Step 2 : Barycentric Correction

At this stage, we must do a barycentric correction on our FITS eventfile. What is barycentric correction and why is it necessary?

All our timing analysis is done assuming that the pulsar signal was sent from a source in an inertial frame and was detected by a receiver in an inertial frame. However, this is not

true. Our detectors are in orbit around the earth, and by extension, around the sun, and are in the gravitational potential well of both these objects. In the same way, our pulsar source is also in some gravitational potential well and isn't an inertial frame. This causes the photons from the source to experience a Shapiro delay due to General Relativistic effects. To counter this, we assume the solar system to be an inertial frame, and transform the time parameter to account for these GR effects and to mimic a situation wherein the detector would be at the solar system's barycenter. In addition to these GR corrections, a large correction must also be made for the doppler motion of the detector due to its orbit around the earth.

Using the code as1bary written by Dipankar Sir and available on the astrosat-ssc website, we will perform a barycentric correction on our eventfile. It is important to note that for this we will require an orbit file, which is a FITS file containing information regarding the orbital motion of Astrosat,and the orbit file must have a few extra row entries from a few seconds before the Tstart of our observation, upto a few seconds after Tstop. From this new event file thus generated, and using the GTI file from earlier, we must then generate the lightcurves, the spectra, and the background spectra.

7.5 Step 3 : Use the spectra/lightcurves

First, as a check, we must generate lightcurves with 1 second timebins and plot them to make sure that our GTI files are working. This is especially helpful for cases like in our Obs ID 620 files, which had faulty GTI files, and had to be modified.

7.5.1 Do a spectral fitting

Spectral fitting can allow us to understand several parameters in a pulsar system. We could either do the fit to the entire spectra, or take certain sections of energy, time, phase etc. as required.

Using XSPEC, we have fitted a simple power law to our Crab spectra. This gives us the photon index and the normalisation factor for our observation. However, it is only possible

to fit a simple power law to our Crab spectra as we are within the 3-80 keV range (for our uses,we have taken only 8-80 keV energy range,because we can use SXT data for the lower energies). For higher energies, it gets a little more complicated because the spectra follow a broken power law trend.

For more complex systems, we can extract more information from spectral fitting like disk temperature, reflection coefficient of the disk, optical depth of the disk, the temperature of electrons in the disk etc., depending on what the behaviour of the object is like. In figures 2.1, we can see an example fit to obs id 620 spectra and the fitting parameters. (fits are done on LAXPC20 spectra)

7.5.2 Lightcurves

Lightcurves provide important information regarding pulse features and doppler motion of the pulsar, and several basic characteristics regarding the kinematic properties of the pulsar and its companion. Spectral fitting can allow us to understand several parameters in a pulsar system. We could either do the fit to the entire spectra, or take certain sections of energy, time, phase etc. as required.

For the purpose of finding the period of the pulse for Crab, we can have 3 methods :
1. Wavelet analysis : In this method, a template wavelet is assumed to be the shape of the pulse and is fitted to our lightcurve data. The parameters of the fit reveal the periodicity and nature of the pulse. However, this method requires prior knowledge of the exact form the pulse takes, which may be a complex cocktail of functions, and also requires a high signalto noise ration in the data which may not be always achievable.

2. Fourier transform : Performing a Fourier transform on the lightcurve gives us a plot in frequency, where the harmonics of the periodic signal can be seen clearly. However,it may not always be feasible to perform a Fourier Transform on the lightcurve. As an example, I have appended the fourier transform of the lightcurve for obs id 620 in Fig 2.2.

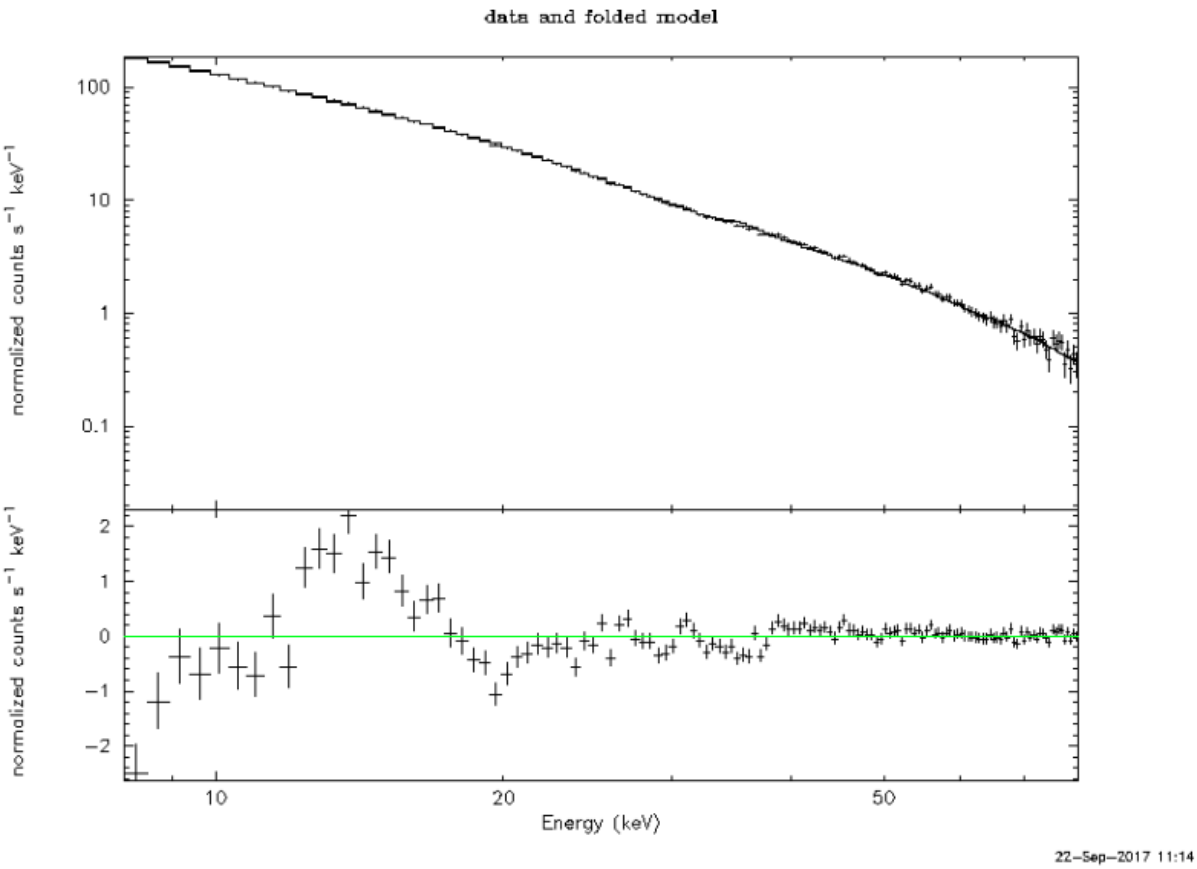


```
=========================================================================
Model powerlaw<1> Source No.: 1   Active/On
Model Model Component  Parameter  Unit     Value
 par  comp
   1    1   powerlaw   PhoIndex            2.10246      +/-  3.91511E-03
   2    1   powerlaw   norm                8.02110      +/-  0.102188
_________________________________________________________________________


Fit statistic : Chi-Squared =          93.84 using 103 PHA bins.

Test statistic : Chi-Squared =          93.84 using 103 PHA bins.
 Reduced chi-squared =         0.9292 for    101 degrees of freedom
 Null hypothesis probability =   6.803473e-01
```

Figure 7.1: Spectral fitting for obs id 620, and Parameters for fit to obs id 620 (background systematic error 5%, Model systematic error 2%

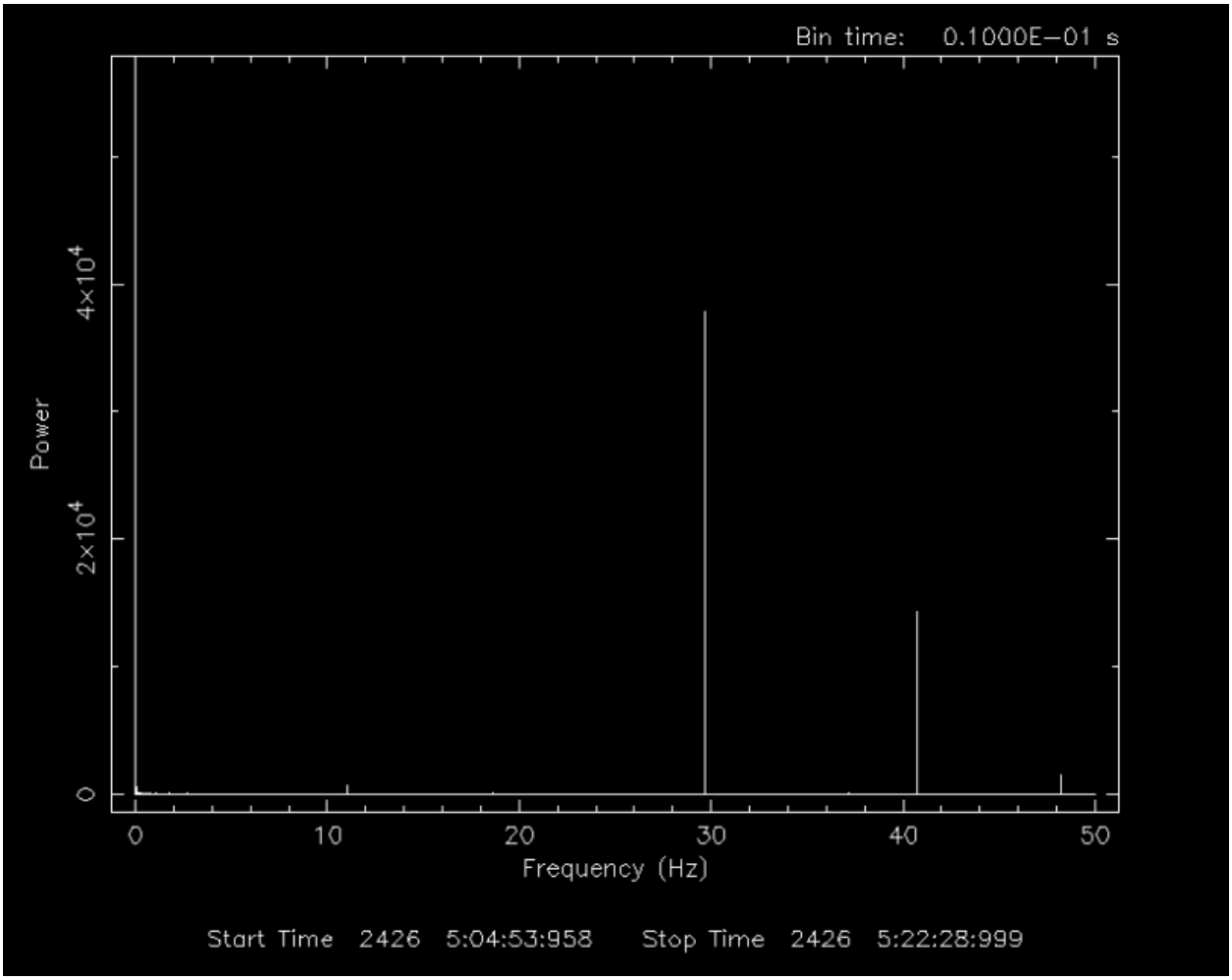

Figure 7.2: Power spectrum for Crab

3. Epoch folding : From Fig 2.2, we can roughly estimate the period of the Crab pulsar.We will feed this information into the module efsearch,which will do an epoch folding search on the lightcurve. What this essentially means is that the efsearch module will attempt to fold the lightcurve in on itself for all periodic units in the lightcurve. It will vary the period within a certain range given by us,and find the most likely period for the lightcurve. We do an efsearch on Crab obs id 620 lightcurve, and the result is shown in Fig 2.3.

Once we have determined a period using efsearch, we can plug it into the efold module which will give us the results of epoch folding a lightcurve. (Fig 2.4)

The pulses are quite broad in this particular folded lightcurve, which tells us something

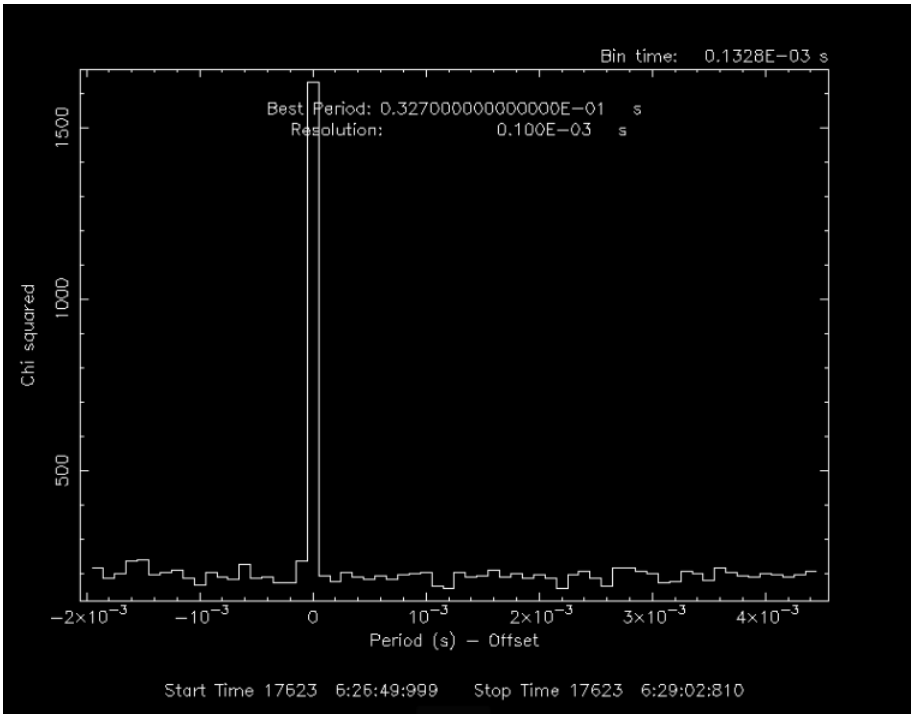

Figure 7.3: Result of efsearch for Crab

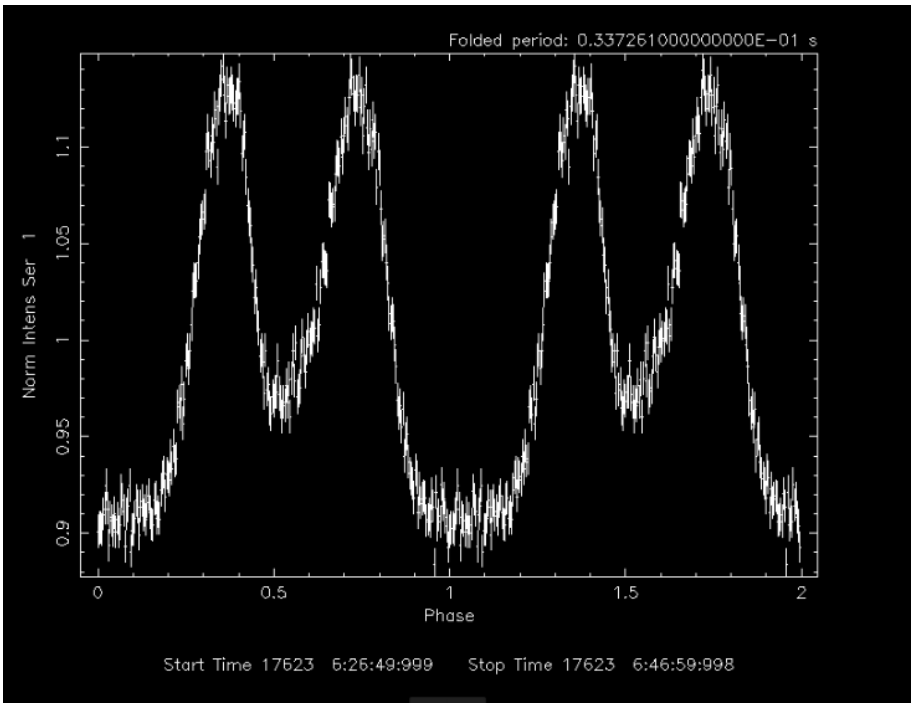

Figure 7.4: Epoch folded lightcurve for Crab

is wrong. In fact, in this entire process, we have assumed that the object does not vary over the course of our observations and the periodic pulses can be perfectly layered on each other. However this is not true.

7.5.3 Phase resolved spectroscopy

Crab pulsar loses angular momentum due to stellar winds and radiation losses. As a result, it slows down by approximately 36 ns every day. This has to be taken into consideration when we want to generate the pulse profile.

Phase is defined as
$\phi = \nu(t - t_0) + \frac{1}{2}\dot{\nu}(t - t_0)^2 + \frac{1}{6}\ddot{\nu}(t - t_0)^3$
where t_0 is the arrival time of the first peak in the radio band (MJD format)
$\nu, \dot{\nu}$ and $\ddot{\nu}$ are the frequency, and the first and second derivative of the frequency respectively. These values are obtained from the Jodrell Bank Ephemeris, which maintain catalogues of Crab variability observations in the radio band.

We consider only the fractional part of the phase, and calculate it for each point in our event file. Each point in time now has a phase attributed to it,that lies between 0 and 1. If we generate a histogram of the phases, we will get the pulse profile. We can now use this profile to identify the different parts of the pulse, and isolate each part of the pulse to study its temporal and spectral characteristics independently. This is known as phase resolved spectroscopy.

Bibliography

[1] L. Bildsten, D. Chakrabarty, J. Chiu, M. H. Finger, D. T. Koh, R. W. Nelson, T. A. Prince, B. C. Rubin, D. M. Scott, M. Stollberg, B. A. Vaughan, C. A. Wilson, and R. B. Wilson, "Observations of accreting pulsars," *The Astrophysical Journal Supplement Series*, vol. 113, pp. 367–408, dec 1997.

[2] S. H. Pravdo and P. Ghosh, "An orbital light-curve model for gx 3012," *The Astrophysical Journal*, vol. 554, no. 1, p. 383, 2001.

[3] N. Sato, F. Nagase, N. Kawai, R. L. Kelley, S. Rappaport, and N. E. White, "Orbital elements of the binary X-ray pulsar GX 301-2," , vol. 304, pp. 241–248, May 1986.

[4] E. Göğüş, I. Kreykenbohm, and T. M. Belloni, "Discovery of a peculiar dip from GX 301-2," , vol. 525, p. L6, Jan. 2011.

[5] V. Doroshenko, A. Santangelo, V. Suleimanov, I. Kreykenbohm, R. Staubert, C. Ferrigno, and D. Klochkov, "Is there a highly magnetized neutron star in GX 301–2?," *Astronomy and Astrophysics*, vol. 515, p. A10, may 2010.

[6] K. Jahoda, C. B. Markwardt, Y. Radeva, A. H. Rots, M. J. Stark, J. H. Swank, T. E. Strohmayer, and W. Zhang, "Calibration of the rossi x-ray timing explorer proportional counter array," *The Astrophysical Journal Supplement Series*, vol. 163, no. 2, p. 401, 2006.

[7] J. K. Blackburn, "FTOOLS: A FITS Data Processing and Analysis Software Package," in *Astronomical Data Analysis Software and Systems IV* (R. A. Shaw, H. E. Payne, and J. J. E. Hayes, eds.), vol. 77 of *Astronomical Society of the Pacific Conference Series*, p. 367, 1995.

[8] "Ftools: The futils sub-package." http://heasarc.gsfc.nasa.gov/ftools/.

[9] "Rxte gof: Rxte archive." https://heasarc.gsfc.nasa.gov/docs/xte/archive.html.

[10] "Creating xte filter files." https://heasarc.gsfc.nasa.gov/docs/xte/recipes/xtefilt.html.

[11] "Rxte gof: History of pca." https://heasarc.gsfc.nasa.gov/docs/xte/whatsnew/big.html.

[12] "Rxte : Creating bitmasks." https://heasarc.gsfc.nasa.gov/docs/xte/recipes/layers.html.

[13] Ş. Şahiner, S. Ç. İnam, and A. Baykal, "A comprehensive study of RXTE and INTEGRAL observations of the x-ray pulsar 4u 190709," *Monthly Notices of the Royal Astronomical Society*, vol. 421, pp. 2079–2087, feb 2012.

[14] S. P. Drave, A. J. Bird, L. Sidoli, V. Sguera, V. A. McBride, A. B. Hill, A. Bazzano, and M. E. Goossens, "INTEGRAL and XMM–newton observations of IGR j16418-4532: evidence of accretion regime transitions in a supergiant fast x-ray transient," *Monthly Notices of the Royal Astronomical Society*, vol. 433, pp. 528–542, may 2013.

[15] J. Wilms, "The magnetospheres of (accreting) neutron stars," *EPJ Web of Conferences*, vol. 64, p. 06001, 2014.

[16] F. Fürst, S. Suchy, I. Kreykenbohm, L. Barragán, J. Wilms, K. Pottschmidt, I. Caballero, P. Kretschmar, C. Ferrigno, and R. E. Rothschild, "Study of the many fluorescent lines and the absorption variability in GX 301-2 withXMM-newton," *Astronomy & Astrophysics*, vol. 535, p. A9, oct 2011.

[17] N. Shakura, K. Postnov, and L. Hjalmarsdotter, "On the nature of 'off' states in slowly rotating low-luminosity x-ray pulsars," *Monthly Notices of the Royal Astronomical Society*, vol. 428, pp. 670–677, oct 2012.

[18] K. A. . R. D. Frank, J., *Accretion Power in Astrophysics*. 2002.

[19] E. Kuulkers, R. Wijnands, T. Belloni, M. Méndez, M. van der Klis, and J. van Paradijs, "Absorption Dips in the Light Curves of GRO J1655-40 and 4U 1630-47 during Outburst," , vol. 494, pp. 753–758, Feb. 1998.

[20] R. Walter, A. A. Lutovinov, E. Bozzo, and S. S. Tsygankov, "High-mass x-ray binaries in the milky way," *The Astronomy and Astrophysics Review*, vol. 23, aug 2015.

[21] M. M. Romanova, A. K. Kulkarni, and R. V. E. Lovelace, "Unstable disk accretion onto magnetized stars: First global three-dimensional magnetohydrodynamic simulations," *The Astrophysical Journal Letters*, vol. 673, no. 2, p. L171, 2008.

[22] M. M. Romanova, A. K. Kulkarni, and R. V. E. Lovelace, "Unstable disk accretion onto magnetized stars: First global three-dimensional magnetohydrodynamic simulations," *The Astrophysical Journal*, vol. 673, pp. L171–L174, jan 2008.

[23] P. Esposito, G. L. Israel, L. Sidoli, A. Tiengo, S. Campana, and A. Moretti, "The x-ray emission of the high-mass x-ray binary IGR j17200-3116," *Monthly Notices of the Royal Astronomical Society*, vol. 441, pp. 1126–1133, may 2014.